Supporting Information For

Molecular insights into the Microscopic Behavior of CO_2 Hydrates in Oceanic Sediments: Implications for Carbon Sequestration

Fengyi Mi[†,‡], Wei Li[†], Jiangtao Pang[†], Othonas A. Moultos[‡], Fulong Ning[*,†], Thijs J.H. Vlugt[*,‡]

[†]National Center for International Research on Deep Earth Drilling and Resource Development, Faculty of Engineering, China University of Geosciences, Wuhan, Hubei 430074, China

[‡]Engineering Thermodynamics, Process & Energy Department, Faculty of Mechanical Engineering, Delft University of Technology, Leeghwaterstraat 39, Delft, 2628CB, the Netherlands

[*]Authors to whom correspondence should be addressed. nflzx@cug.edu.cn, t.j.h.vlugt@tudelft.nl

Total number of pages: 34

Total number of figures: 41

Total number of tables: 2

Total number of videos: 4

Contents of Supporting Information

Supporting Videos

Supporting Reference

Additional Details for Simulation Models and Methods

Simulation Models

The illite unit cell was obtained by modifying the pyrophyllite unit cell taken from the United States Mineral Crystal Structure Database[1]. To construct the illite crystal structure with the chemical formula $K_1(Si_7Al)Al_4O_{20}(OH)_4$, a Si atom in the pyrophyllite unit cell was substituted with an Al atom. An illite layer is created by replicating the illite unit cell (24 × 8 × 1). An illite nanopore consists of two identical illite layers, and the nanopore size was set to 46 Å. CO_2 hydrate belongs to SI-type hydrate, mainly composed of 5^{12} and $5^{12}6^2$ cages. A standard CO_2 hydrate crystal (2 × 6 × 4) was inserted into the middle region of the illite nanopore. The CO_2 hydrate crystal contains 288 CO_2 and 1656 H_2O molecules, and the size was 24.3 × 72.3 × 36.3 Å in the xyz directions. An aqueous homogeneous solution was also inserted into the illite nanopore. The homogeneous solution contains 1277 CO_2, 7340 H_2O, 82 Na^+, 82 Cl^-, and 192 K^+. 82 Na^+ and Cl^- resulting in a salinity of 3.5 wt%, which is close to real seawater. Two layers of illite clay generate 384 negative charges through isomorphic substitution. Therefore, we added 384 K^+ to compensate for the negative charge generated by the illite clay surfaces. It is worth noting that the 384 K^+ are evenly divided into two parts: (1) the homogeneous solution and (2) outside the illite nanopore. This avoids extreme salt concentrations in the illite nanopore. A 5 Å buffer layer was placed between the CO_2 hydrate crystal and the illite clay layer, which eliminates the interaction between the illite surface and the CO_2 hydrate crystal in the initial configuration. Different numbers of urea molecules were inserted into the illite nanopores to represent different urea concentrations (1.6wt%, 3 wt%, 4.5 wt%, and 6 wt%). This allows for a precise analysis of the interaction between urea and geofluid. Too high a urea concentration will result in an aggregate phase between urea and geofluid, while too low a concentration will not reveal the role of urea in the growth and dissociation of CO_2 hydrates, and mechanical instability of CO_2 hydrate-illite interface in the brine-urea-illite system. A system without urea molecules was simulated as a control system. Each simulation system contains about 60,000 atoms. The dissociation of CO_2 hydrate was simulated by increasing the temperature to 307 K. High temperatures can promote hydrate dissociation in a short time and save calculation costs[2]. All force field parameters for H_2O, CO_2, ions, illite, and urea molecules in the systems are shown in Table S2.

Table S1. Number of molecules of each species for the five different simulations.

	simulation systems in illite silt-nanopore					
System	N_{CO_2}	N_{H_2O}	N_{K^+}	N_{Na^+}	N_{Cl^-}	N_{urea}
$H_{0\%Urea}$	1565	8996	384	82	82	0
$H_{1.6\%Urea}$	1565	8996	384	82	82	64
$H_{3\%Urea}$	1565	8996	384	82	82	127
$H_{4.5\%Urea}$	1565	8996	384	82	82	191
$H_{6\%Urea}$	1565	8996	384	82	82	254

Table S2. Parameters for the TIP4P/ice water model[3], TraPPE CO_2[4], OPLS-AA urea[5], and the CLAYFF force field[6]. σ and ε are the Lennard-Jones parameters, in units of nm and kJ/mol, respectively; q is the partial charge of an atom in units of elementary charge (e); m is the atomic mass in units of g/mol.

atom	ε / [kJ/mol]	σ / [nm]	q / [e]	m / [g/mol]
H_2O				
O (MW)	0	0	-1.1794	0
O	0.8822	0.31668	0	16
H	0	0	0.5897	1.008
CO_2				
C	0.224478	0.28	0.70	12.011
O	0.656806	0.305	-0.35	15.9994
O (OM)	0	0	0	0
Ion				
Cl	0.418998	0.439997	-1.0	35.453
Na	0.544572	0.235002	1.0	22.989
K	0.41858	0.333401	1.0	39.0983
Illite				
Si (st)	7.70065×10^{-6}	0.3302	2.1	28.09
Al (ao)	5.56388×10^{-6}	0.4271	1.575	26.98
Al (at)	7.70065×10^{-6}	0.3302	1.575	26.98
O (ob)	0.65017	0.316556	-1.05	16
O (obts)	0.65017	0.316556	-1.1688	16
O (oh)	0.65017	0.316556	-0.95	16
H (ho)	0	0	0.425	1.008
Urea				
C	0.43932	0.375	0.142	12.011
O	0.87864	0.296	-0.39	15.999
N	0.71128	0.325	-0.542	14.007
H	0	0	0.333	1.008

Wall Methods

In the simulation box, the upper and lower clay layers will interact (*i.e.*, stacking) with each other due to the periodicity in the z direction, which will inevitably affect the structure and stability of the clay layer and even the surface properties of the illite. Therefore, we do not set the periodicity in the z direction and use two layers of virtual walls to limit interactions between the upper and lower clay layers. The parameters of the atoms in the virtual walls are as follows: ρ_w = 60 atoms/nm^3, ϵ_w = 1.13 kJ/mol, σ_w = 0.37 nm, and a 9-3 Lennard-Jones potential. The atom type on the virtual wall is the C atom with a charge of 0. In the initial configuration, the length of the simulation box in the z direction is large enough so that there is sufficient distance between the walls and the clay layers. On the isothermal-isobaric *NPT* ensemble, we use a semi-isotropic pressure scaling method to achieve independent scaling in the xy and z directions[7]. The pressure scaling factor in the xy direction is set to 0, and the pressure scaling factor in the z direction is set to 4.5×10^{-5}. The simulation box only compresses the z direction to achieve the given pressure value. In all simulations, the distance between the wall and the solution was larger than 10 Å, which did not affect the simulation results.

Pull Methods

We apply a constant force to the atoms on the upper illite layer in the z/-z direction for the tensile and compressive simulations. The surface area of the clay layer is about 89.09 nm^2. Therefore, pressure will be generated in the illite nanopores. The constant pull rate is 10 Å/ns. The simulation time is 1 ns, with the trajectory is saved every 1 ps. The illite clay layer is incompressible in the xy direction, and the force acts in the z direction. Therefore, the *NPT* ensemble cannot precisely control the pressure value by compressing the box size. In this study, we use the *NVT* system to control the temperature and use the external force to change the pressure. As a result, an *NVT* ensemble was adopted to perform deformation simulations, with the temperature controlled by the Nosé-Hoover[8] thermostat at 273.15 K. In the deformation period, the interactions of urea molecules, water molecules, CO_2 molecules, and ions in the nanopores will deform CO_2 hydrate crystals.

Simulation Methods

The geometry of the H_2O molecules is maintained by applying the SETTLE algorithm[7]. The Lorentz-Berthelot mixing rules are used for describing the unlike interactions. The equations of motion were integrated according to the leapfrog algorithm with a 2.0 fs timestep. The well depth $\varepsilon_{O(CO_2)\text{-}O(H_2O)}$ between the oxygen in CO_2 and the oxygen in H_2O was scaled by a factor of 1.08. The initial configurations were energy minimized by using the steepest descent algorithm. A pre-equilibrium simulation was performed for 2 ns, and the temperature was set to 250 K by controlling the v-rescale[9] algorithm, and the pressure was 500 bar by the Berendsen[10] algorithm. Growth simulations were performed in the isothermal-isobaric *NPT* ensemble for 2.0 μs at 250 K and 500 bar, and the temperature and pressure were changed to the Nosé-Hoover[8] thermostat and Parrinello-Rahman[11] barostat,

respectively. At the end of the growth simulation, the dissociation simulation was performed in the isothermal-isobaric *NPT* ensemble for 10 ns at 307 K and 100 bar. The temperature and pressure were also changed to the Nosé-Hoover[8] thermostat and Parrinello-Rahman[11] barostat, respectively. At the end of the growth simulation, the tension and compression simulations were performed in the *NVT* ensemble for 1 ns. To monitor the growth and dissociation of CO_2 hydrates, and mechanical instability of CO_2 hydrate-illite interface in the brine-urea-illite system, the cage analysis algorithm proposed by Jacobson *et al.*[12] is used to identify the seven cage types (5^{12}, $5^{12}6^2$, $5^{12}6^3$, $5^{12}6^4$, $4^15^{10}6^2$, $4^15^{10}6^3$, and $4^15^{10}6^4$). CO_2 hydrate belongs to SI-type hydrate, mainly composed of 5^{12} and $5^{12}6^2$ cages, and its ratio is 1:3.

Calculation principle of the residence time correlation function

The principle of correlation functions is well established and documented in GROMACS 2022[7]. The residence time correlation function is one such function. The definition of the residence correlation function $C_f(t)$ for residence $f(t)$ is:

$$C_f(t) = \left\langle f(\xi) f(\xi + t) \right\rangle_\xi \tag{1}$$

$\left\langle \ \right\rangle$ indicates averaging over ξ, which is over time origins.

The residence time τ is calculated by the numeric integration of the residence correlation function:

$$\tau = \int_0^\infty C_f(t) dt \tag{2}$$

In MD simulations, correlation functions are calculated based on data points with discrete time intervals Δt, so the residence correlation function $C_f(t)$ is:

$$C_f(j\Delta t) = \frac{1}{N-j} \sum_{i=0}^{N-1-j} f(i\Delta t) f((i+j)\Delta t) \tag{3}$$

Where *N* is the number of available time frames for the calculation.

In this study, each τ_{Res} is calculated within 1 ns for CO_2, H_2O, and ions near urea molecules. The GROMACS command *gmx_mpi hbond -ac -contact* can perform the calculation of the residence correlation function.

Calculation principle of the CO_2 hydrate growth rate (R_{HG})

To monitor CO_2 hydrate growth kinetics, the CO_2 hydrate growth rate (R_{HG}) is defined. The F_4 order parameter serves as an effective discriminator for distinguishing the water phase, with average values of -0.04, -0.4, and 0.7 for liquid water, ice, and hydrate, respectively[13]. The F_4 order parameter is defined by

$$F_4 = \langle cos(3\emptyset) \rangle \tag{4}$$

The value of F_4 is computed by the water-water pair as a function of the torsional angle $\emptyset$ between oxygen atoms within 3.5 Å and the outermost hydrogen atoms in the water-water pairs. The R_{HG} value can be used for

monitoring CO_2 hydrate growth kinetics. The R_{HG} is calculated as follows:

$$R_{HG} = \frac{F_4(t+\Delta t)-F_4(t)}{\Delta t} \quad (5)$$

The noise reduction (*i.e.*, smoothing) was used for F_4 function. The slope of the F_4 curve is CO_2 hydrate growth rate R_{HG}.

Calculation principle of the Increments of the number of hydrogen bonds per square nanometer (ΔHbonds)

To assess the changes in the number of hydrogen bonds near the upper illite surface, we define the Increments of the number of hydrogen bonds per square nanometer (ΔHbonds). This increment of the number of hydrogen bonds per square nanometer as a function of mechanical tensile/compressive strain (ε) is:

$$\Delta\text{Hbonds} = \frac{N_{\text{H-bonds}}-N_0}{S_{\text{illite surface}}} \quad (6)$$

Where $N_{\text{H-bonds}}$ is the number of hydrogen bonds between urea/H_2O molecules and the upper illite surface under tensile/compressive strains (ε). N_0 is the number of hydrogen bonds between urea/H_2O molecules and the upper illite surface at $\varepsilon = 0$. In this study, $S_{\text{illite surface}}$ is the surface area of the upper surface of illite, which is 89.09 nm^2.

Calculation principle of the number of hydrogen bonds at different distances from the upper surface (HCD)

We calculated the number of hydrogen bonds at different distances from the upper illite surface. These hydrogen bonds are mainly formed between water molecules. The number of hydrogen bonds was calculated for every 2 Å from the upper illite surface. The VMD software[14] was used to calculate hydrogen bonds. The cut-off length and angle are set to 3.5 Å and 60° respectively in the VMD software.

Supporting Figures

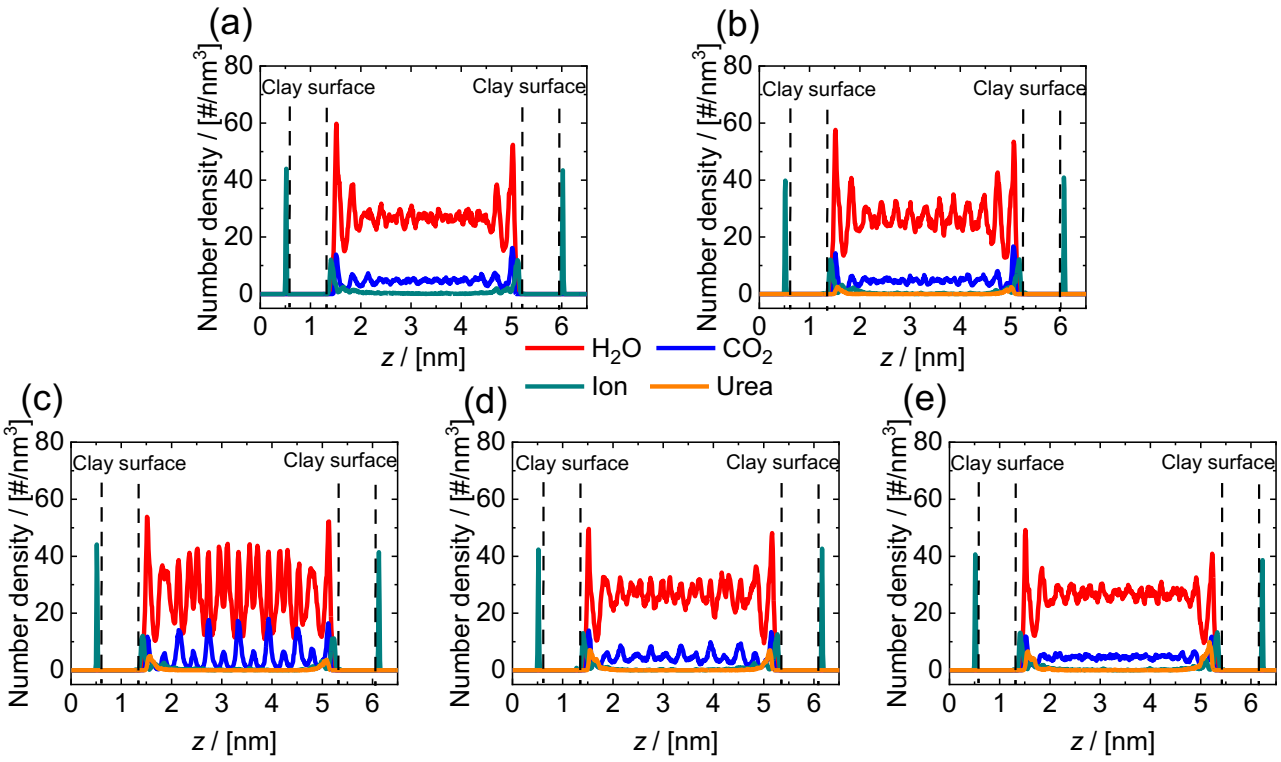

Figure. S1. Number density distribution of H_2O, CO_2, ions, and urea molecules along the z-axis direction for 1.95 - 2.0 μs for the (a) $H_{0\%Urea}$, (b) $H_{1.6\%Urea}$, (c) $H_{3\%Urea}$, (d) $H_{4.5\%Urea}$, and (e) $H_{6\%Urea}$ systems.

We found that the fluctuations of H_2O and CO_2 molecules of the $H_{3\%Urea}$ system are larger than those of other systems, which is attributed to the location difference of CO_2 hydrate. At the end of the simulation, standard CO_2 hydrate crystals are parallel to the xy plane and perpendicular to the z direction in the $H_{3\%Urea}$ system (Figure S16(c)). Sharp, the CO_2 hydrate crystals in other systems are not perpendicular to the z direction (Figure S16(a-e)). Therefore, the number density of H_2O and CO_2 molecules in the z-direction in the $H_{3\%Urea}$ system will fluctuate more than for other systems.

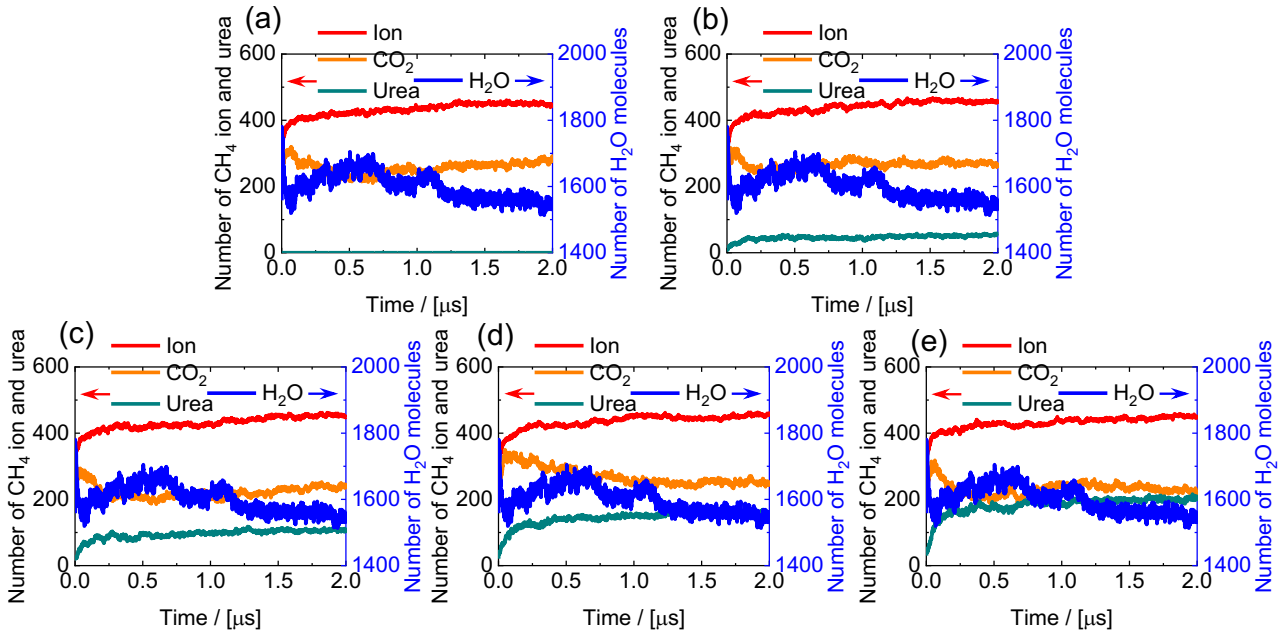

Figure S2. Evolution of the number of ions, CO_2, H_2O, and urea molecules near the illite surface within 5 Å in the (a) $H_{0\%Urea}$, (b) $H_{1.6\%Urea}$, (c) $H_{3\%Urea}$, (d) $H_{4.5\%Urea}$, and (e) $H_{6\%Urea}$ systems.

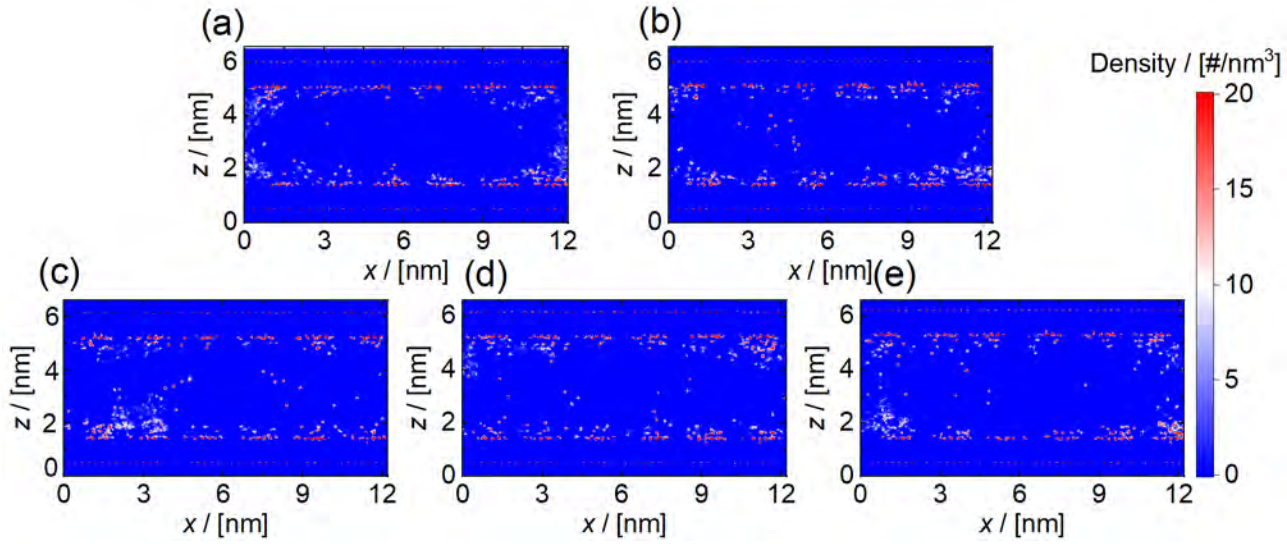

Figure S3. Number density distribution of ions for the last 0.01 μs in the (a) $H_{0\%Urea}$, (b) $H_{1.6\%Urea}$, (c) $H_{3\%Urea}$, (d) $H_{4.5\%Urea}$, and (e) $H_{6\%Urea}$ systems.

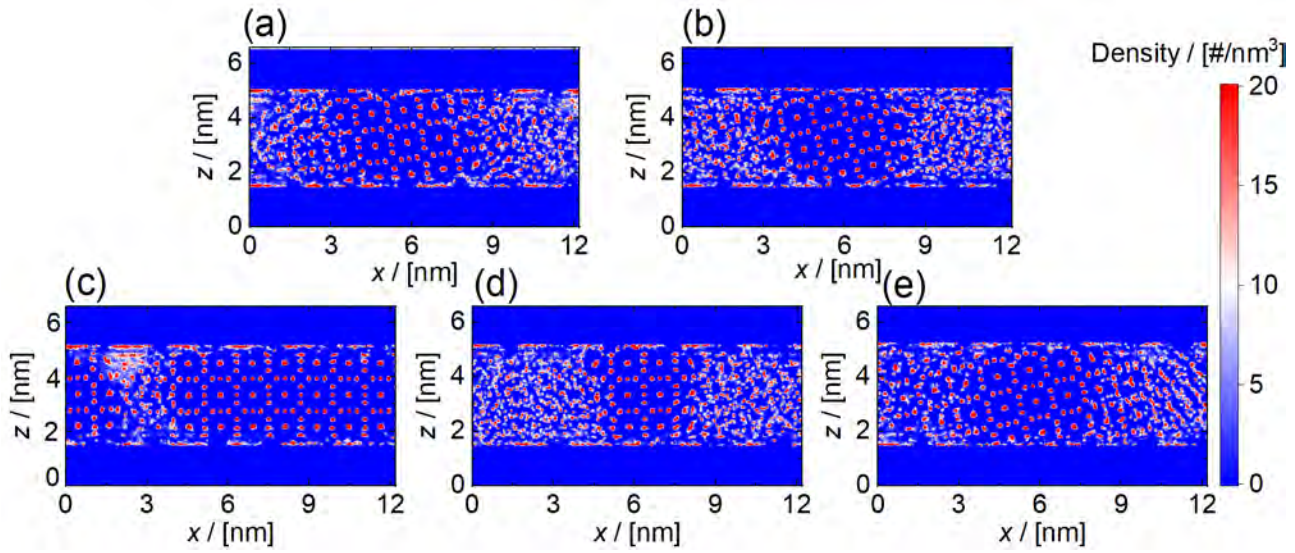

Figure S4. Number density distribution of CO_2 molecules for the last 0.01 μs in the (a) $H_{0\%Urea}$, (b) $H_{1.6\%Urea}$, (c) $H_{3\%Urea}$, (d) $H_{4.5\%Urea}$, and (e) $H_{6\%Urea}$ systems.

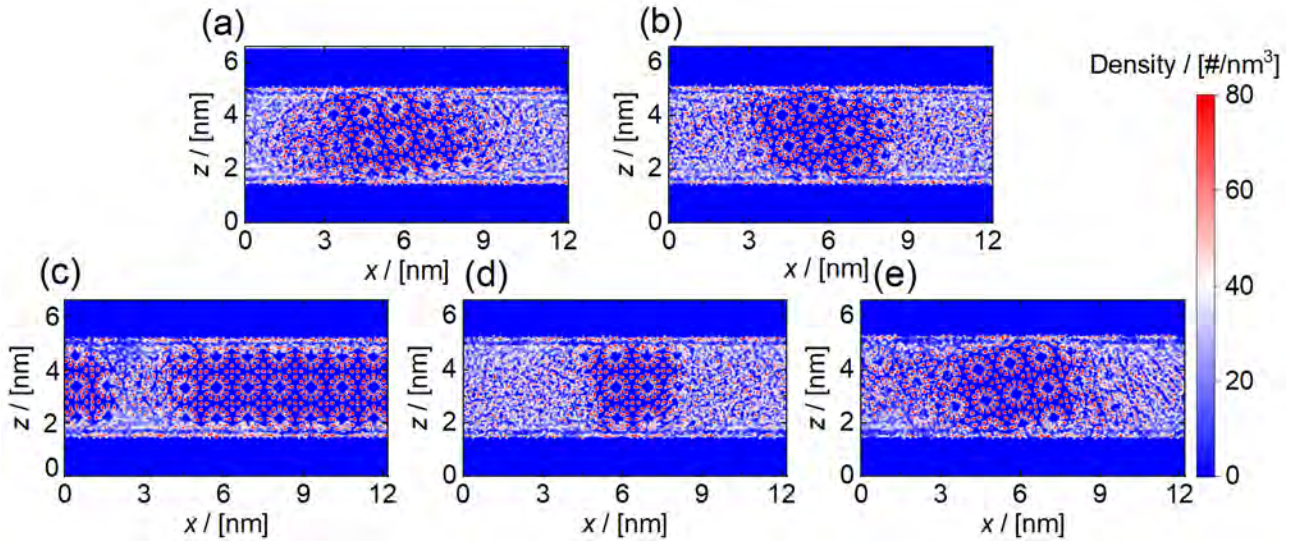

Figure S5. Number density distribution of H_2O molecules for the last 0.01 μs in the (a) $H_{0\%Urea}$, (b) $H_{1.6\%Urea}$, (c) $H_{3\%Urea}$, (d) $H_{4.5\%Urea}$, and (e) $H_{6\%Urea}$ systems.

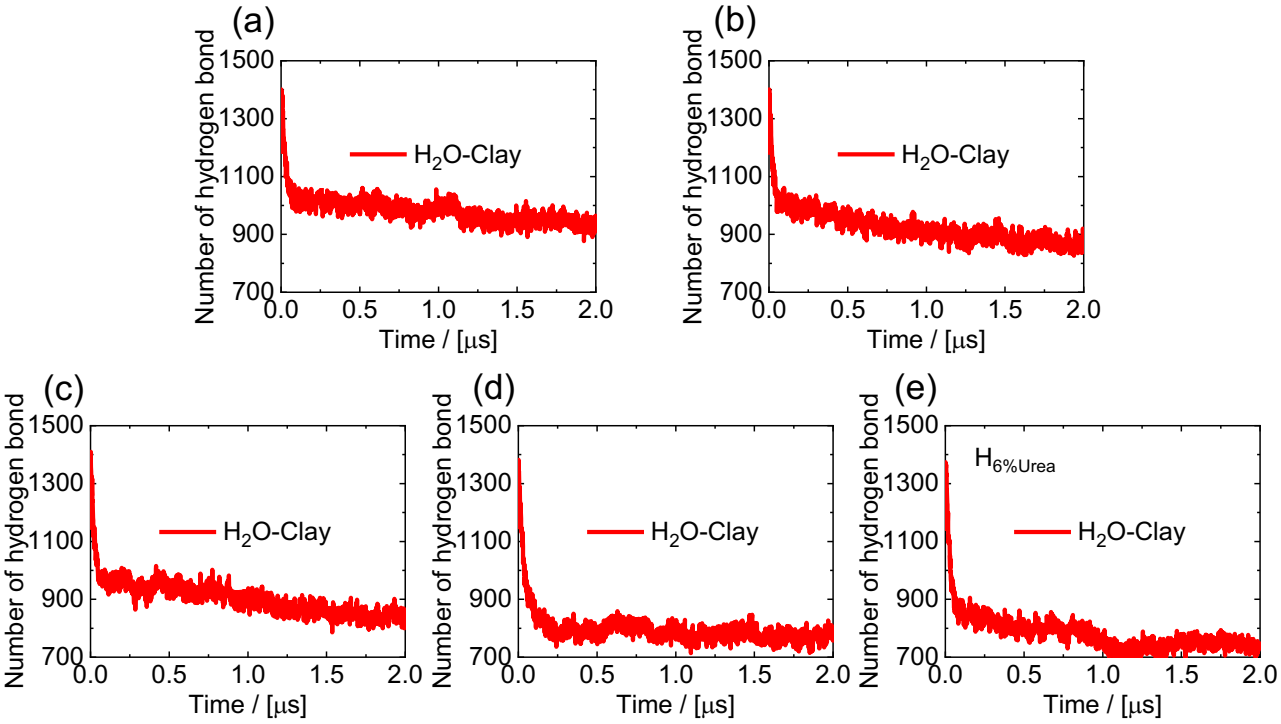

Figure S6. Evolution of the number of hydrogen bonds between the illite surface and H_2O molecules in the (a) $H_{0\%Urea}$, (b) $H_{1.6\%Urea}$, (c) $H_{3\%Urea}$, (d) $H_{4.5\%Urea}$, and (e) $H_{6\%Urea}$ systems.

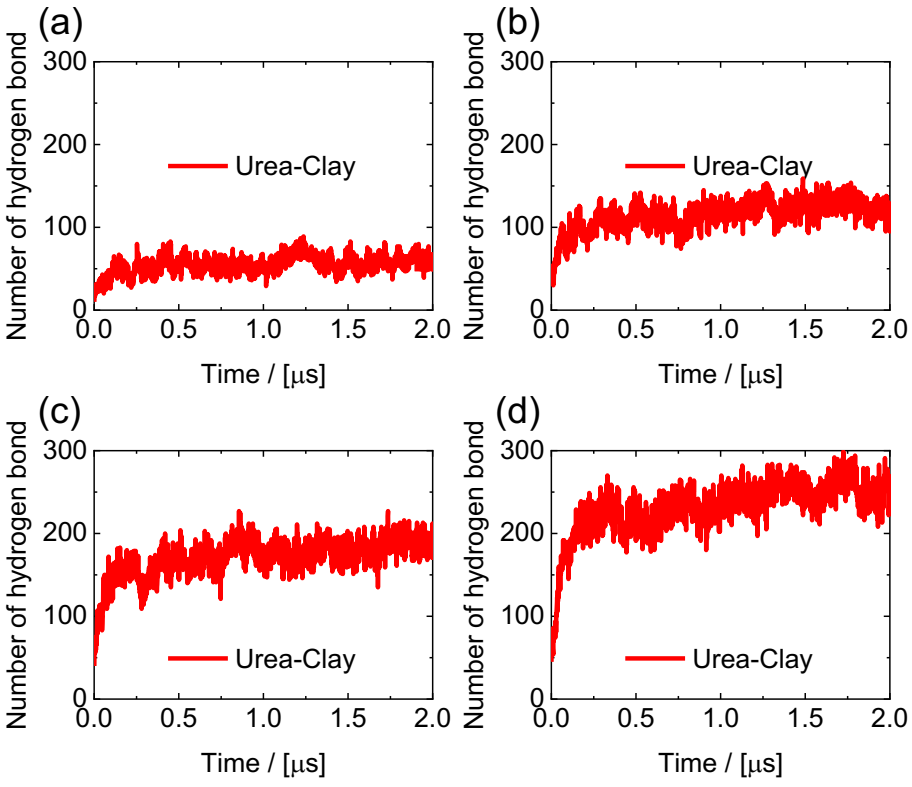

Figure S7. Evolution of the number of hydrogen bonds between the illite surface and urea molecules in the (a)

$H_{1.6\%Urea}$, (b) $H_{3\%Urea}$, (c) $H_{4.5\%Urea}$, and (d) $H_{6\%Urea}$ systems.

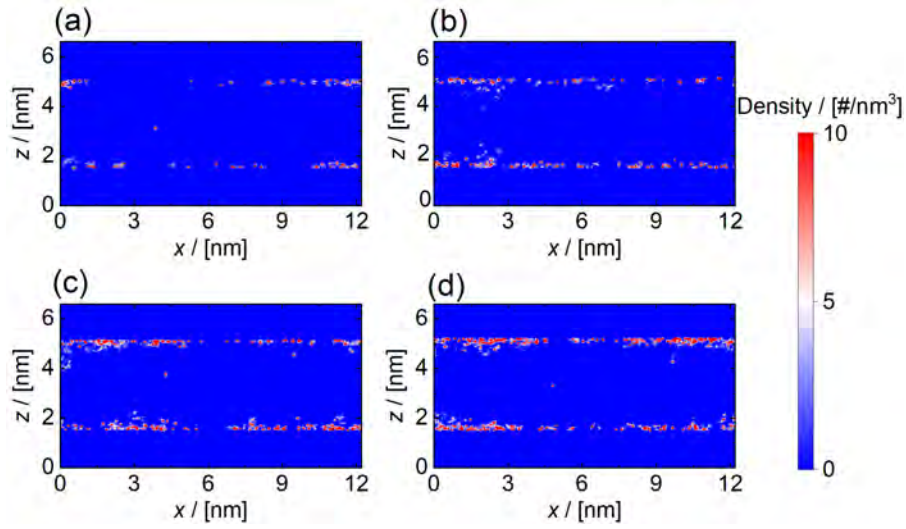

Figure S8. Number density distribution of urea molecules for the last 0.01 μs in the (a) $H_{1.6\%Urea}$, (b) $H_{3\%Urea}$, (c) $H_{4.5\%Urea}$, and (d) $H_{6\%Urea}$ systems.

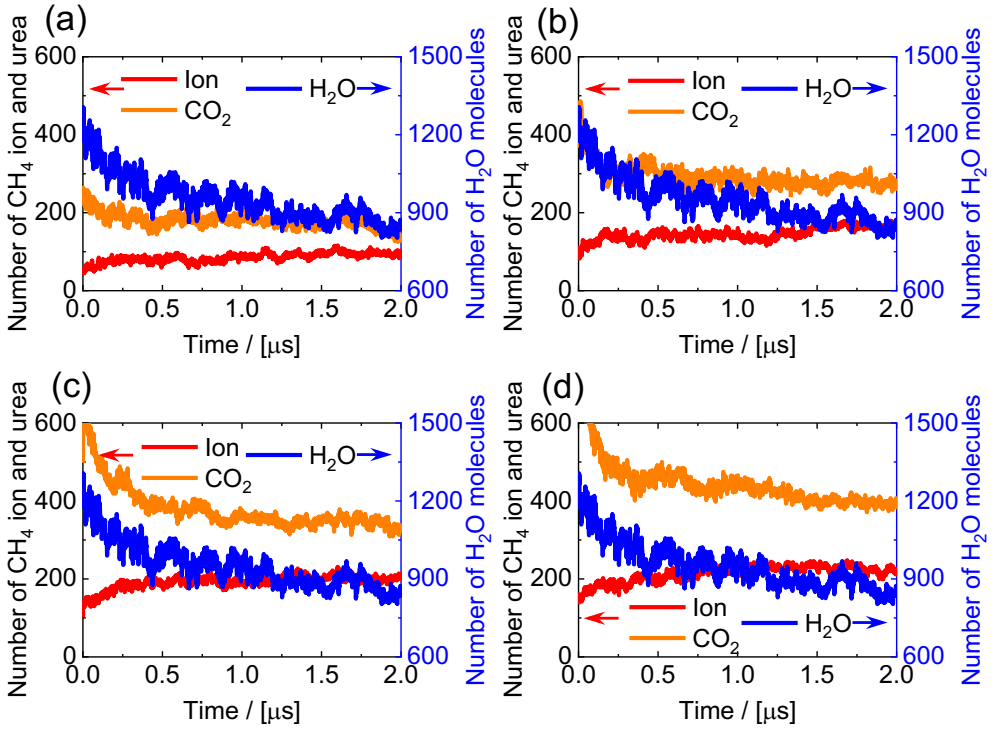

Figure S9. Evolution of the number of ions, CO_2, and H_2O molecules near the urea molecules within 5 Å in the (a) $H_{1.6\%Urea}$, (b) $H_{3\%Urea}$, (c) $H_{4.5\%Urea}$, and (d) $H_{6\%Urea}$ systems.

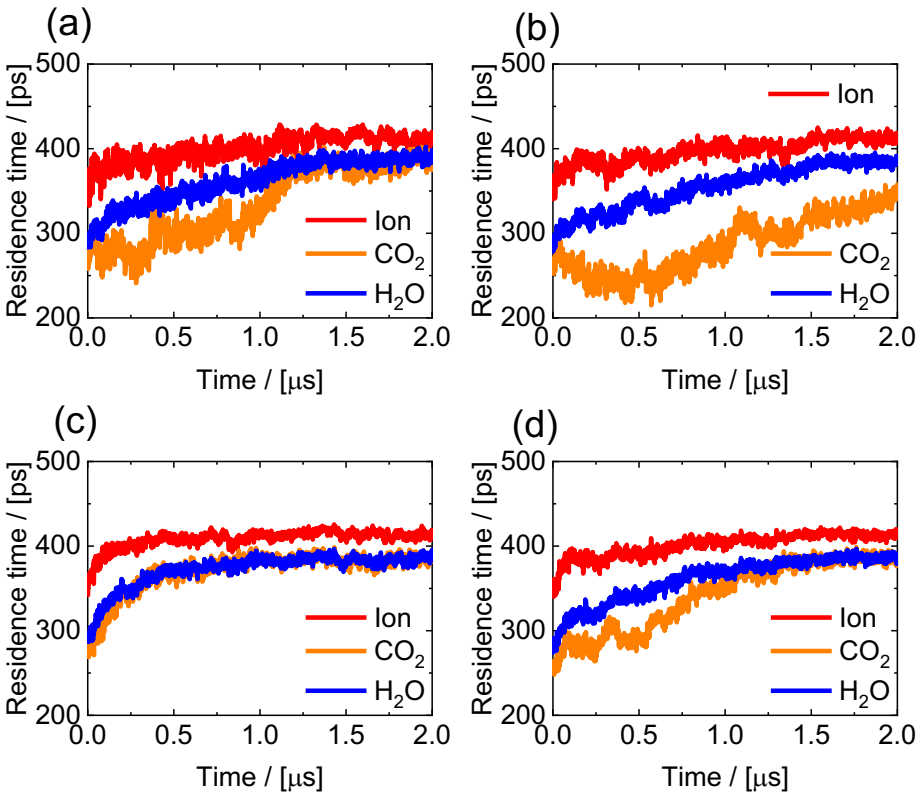

Figure S10. Evolution of the average residence time (τ_{Res}) for H_2O, ions and CO_2 molecules near the urea molecules in the (a) $H_{1.6\%Urea}$, (b) $H_{3\%Urea}$, (c) $H_{4.5\%Urea}$, and (d) $H_{6\%Urea}$ systems.

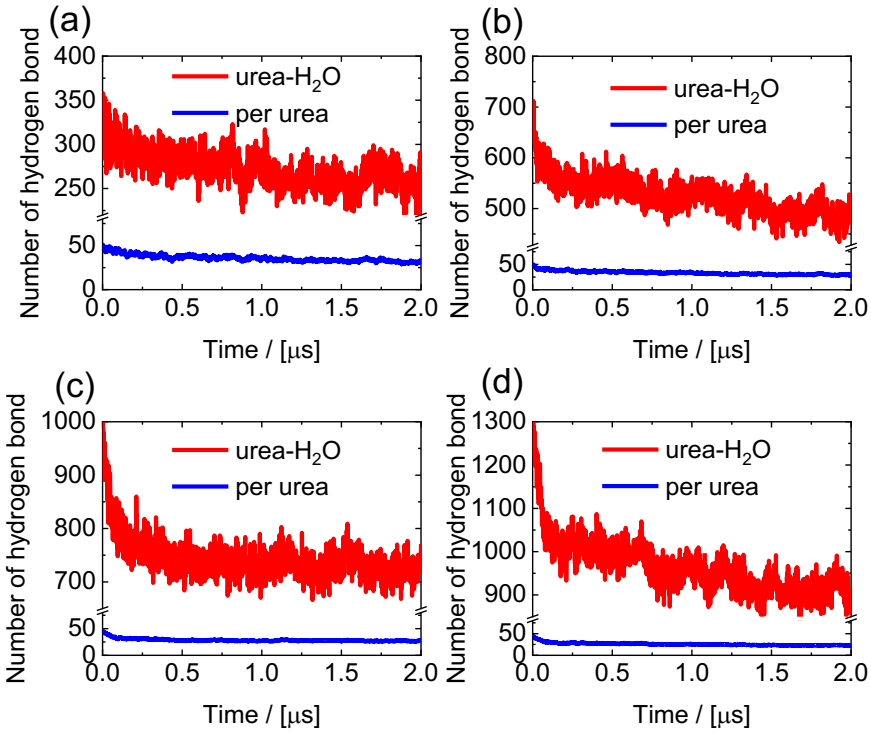

Figure S11. Evolution of the number of hydrogen bonds between urea and H_2O molecules and total hydrogen bonds near per urea molecule within 5 Å in the (a) $H_{1.6\%Urea}$, (b) $H_{3\%Urea}$, (c) $H_{4.5\%Urea}$, and (d) $H_{6\%Urea}$ systems.

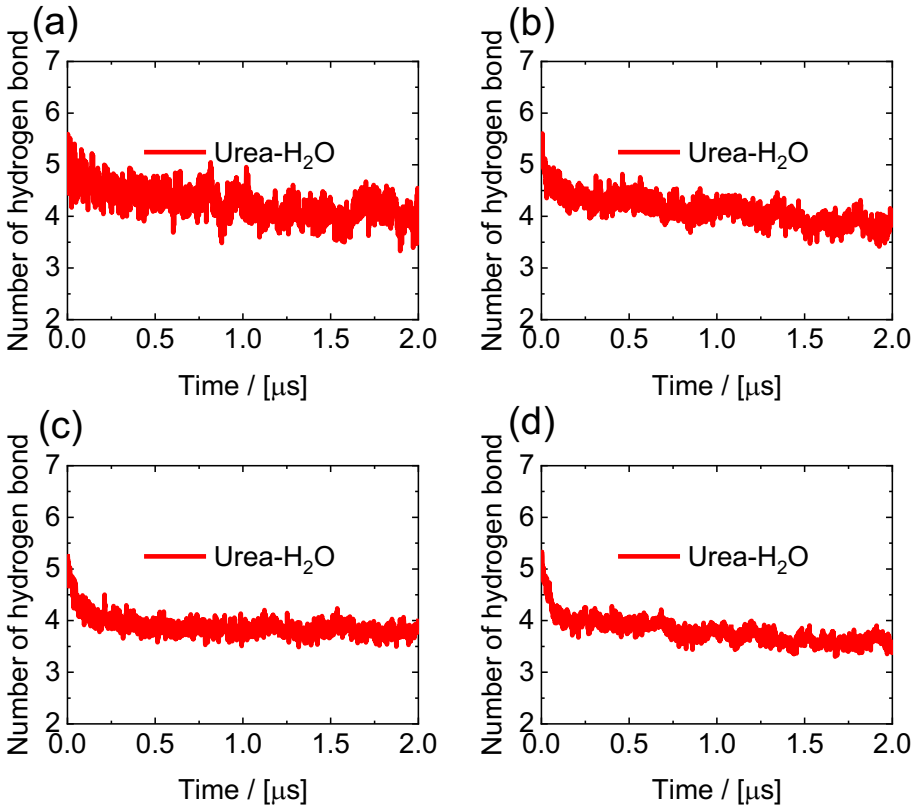

Figure S12. Evolution of the number of hydrogen bonds between per urea molecule and H_2O molecules in the (a) $H_{1.6\%Urea}$, (b) $H_{3\%Urea}$, (c) $H_{4.5\%Urea}$, and (d) $H_{6\%Urea}$ systems.

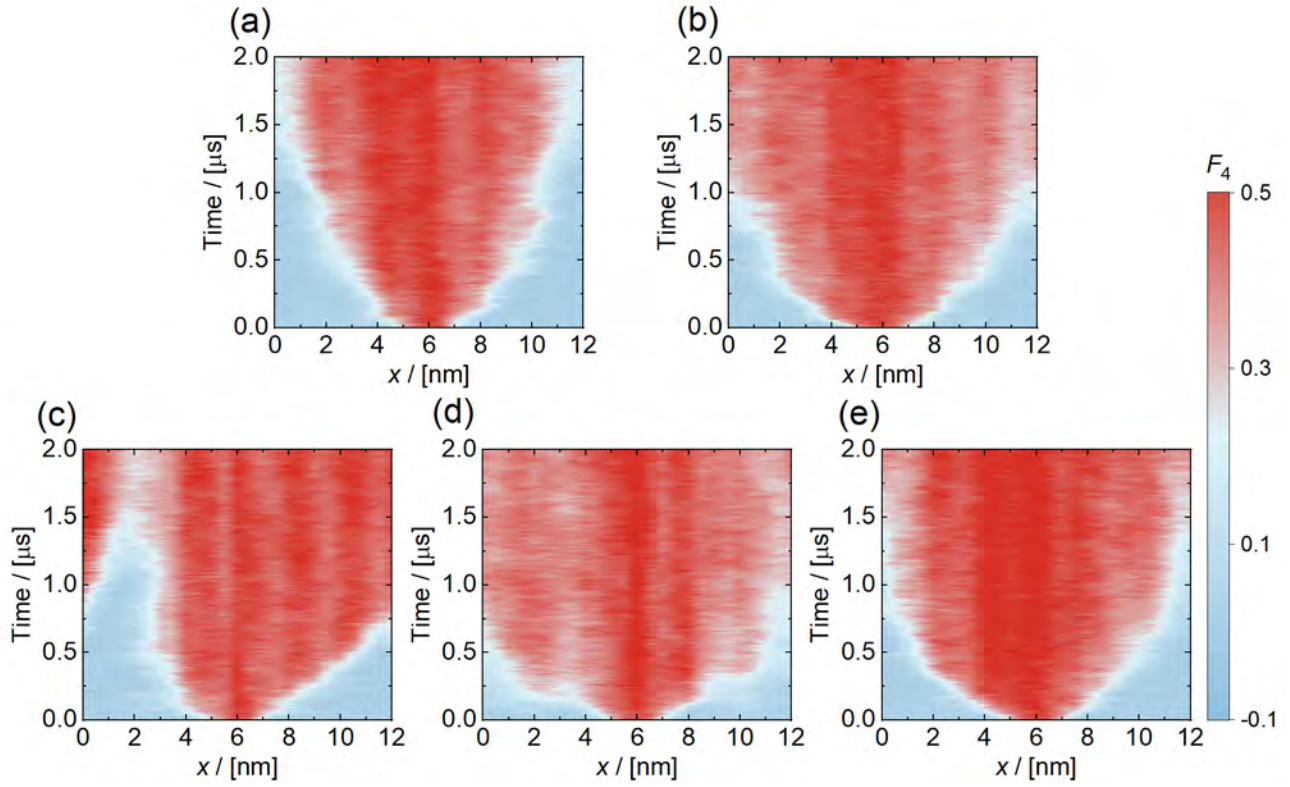

Figure S13. Evolution of the F_4 order parameter along the x-axis in the (a) $H_{0\%Urea}$, (b) $H_{1.6\%Urea}$, (c) $H_{3\%Urea}$, (d) $H_{4.5\%Urea}$, and (e) $H_{6\%Urea}$ systems.

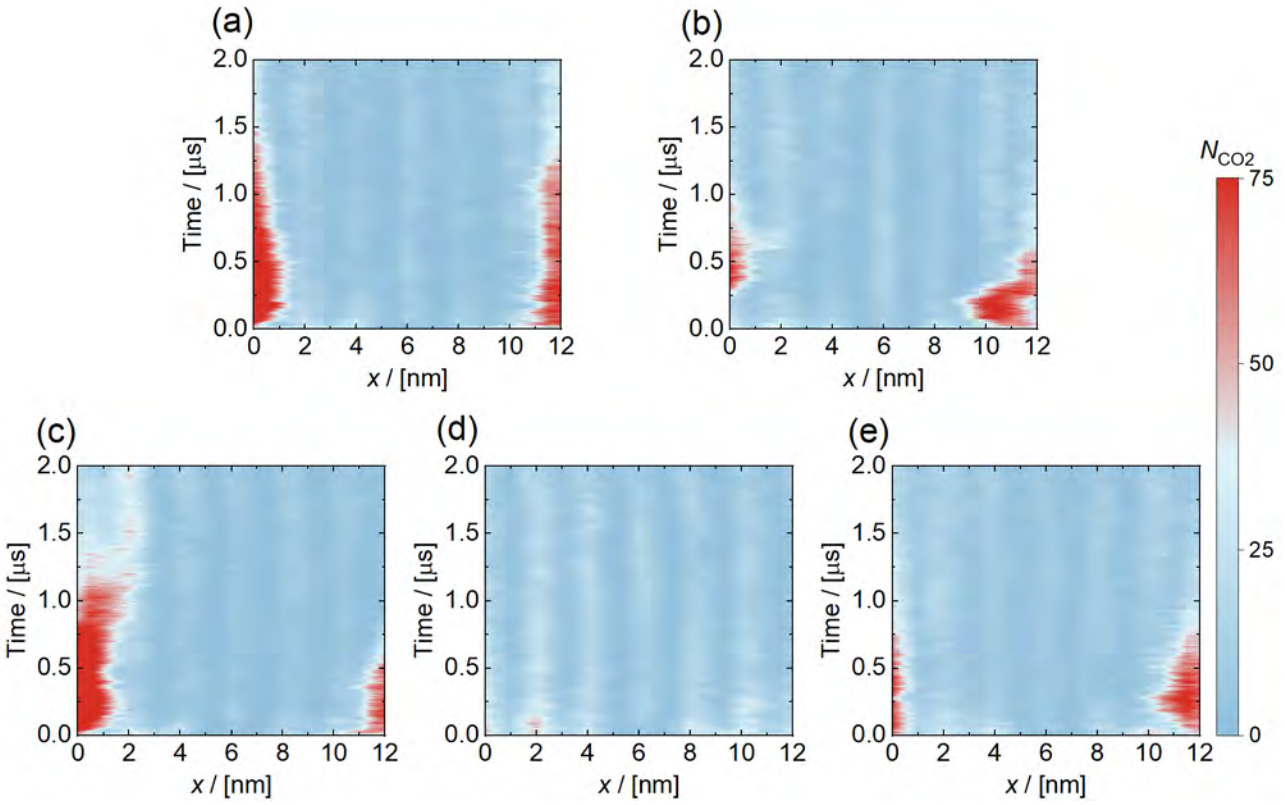

Figure S14. Evolution of the number of CO_2 molecules in the nanobubbles (N_{CO2}) along the x-axis in the (a) $H_{0\%Urea}$, (b) $H_{1.6\%Urea}$, (c) $H_{3\%Urea}$, (d) $H_{4.5\%Urea}$, and (e) $H_{6\%Urea}$ systems.

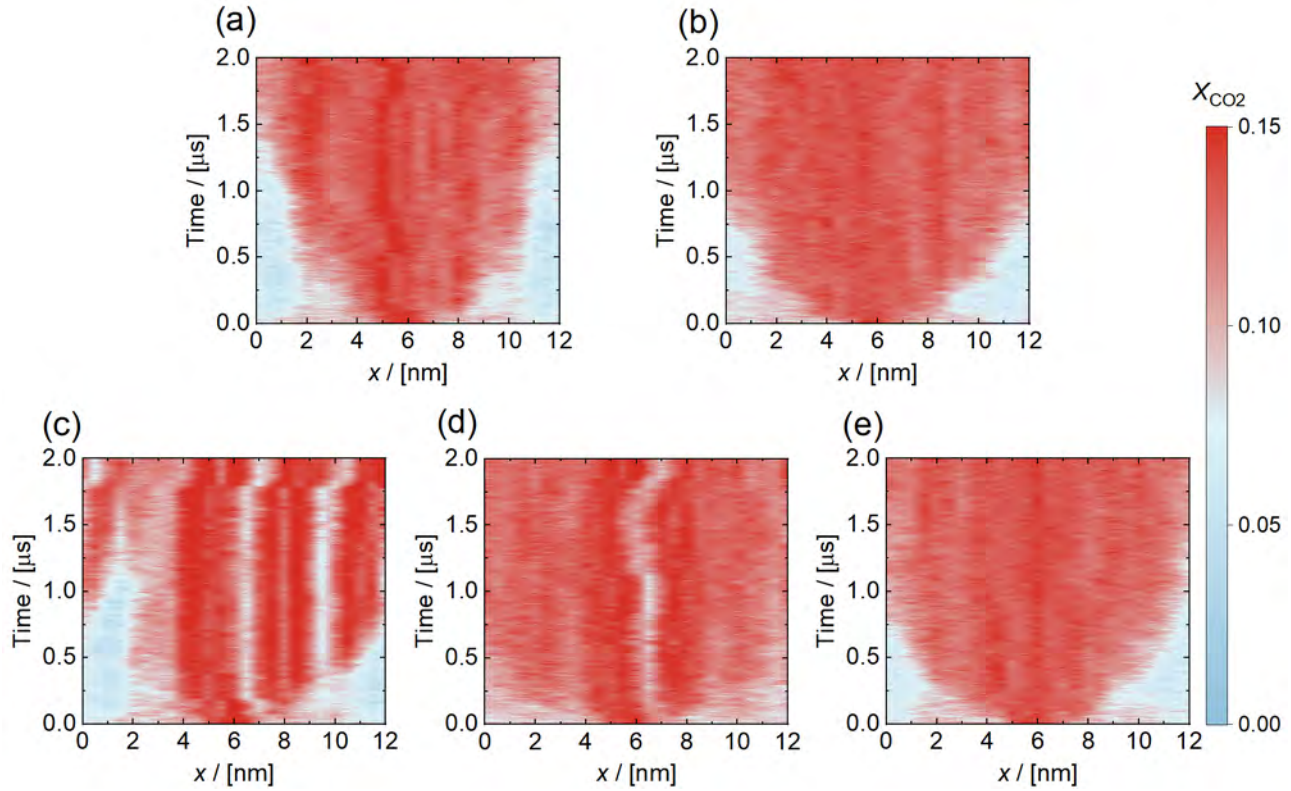

Figure S15. Evolution of the CO_2 mole fraction in water (x_{CO2}) for solutions along the x-axis in the (a) $H_{0\%Urea}$, (b) $H_{1.6\%Urea}$, (c) $H_{3\%Urea}$, (d) $H_{4.5\%Urea}$, and (e) $H_{6\%Urea}$ systems.

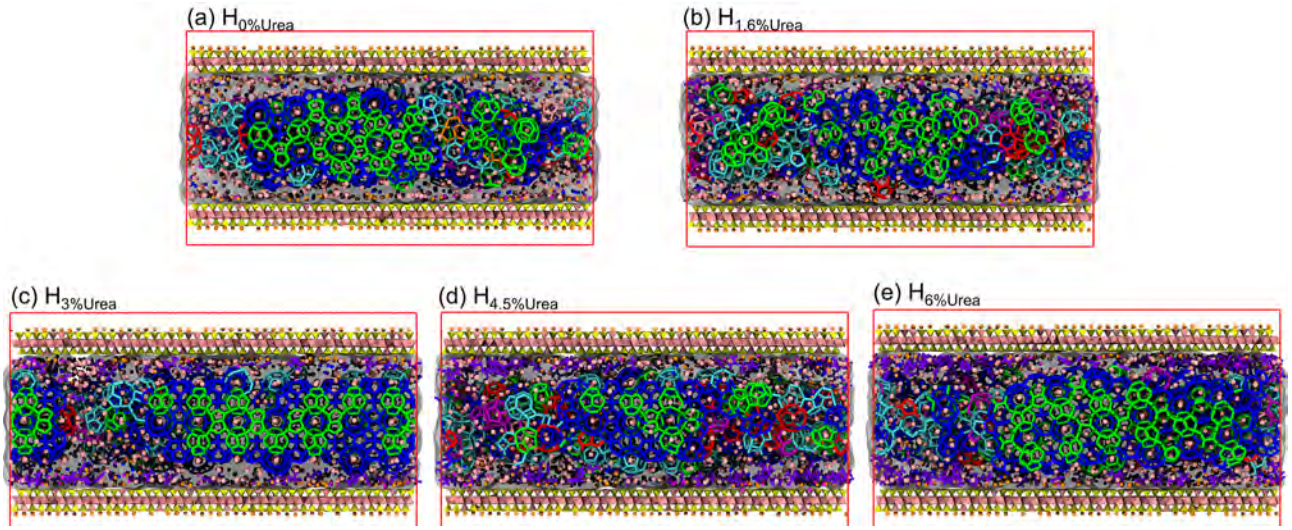

Figure S16. Growth snapshots of CO_2 hydrates formed at the end of the simulation (at 2.0 μs) for the z-x plane in the different simulations: (a) $H_{0\%Urea}$, (b) $H_{1.6\%Urea}$, (c) $H_{3\%Urea}$, (d) $H_{4.5\%Urea}$, and (e) $H_{6\%Urea}$ systems. Illite is displayed as polyhedral, *i.e.,* yellow (Si atom), and pink (Al atom). Pink, blue, magenta, orange, and violet represent CO_2, Cl^-, Na^+, K^+, and urea, respectively. Hydrate cages are shown as sticks in various colors (green for 5^{12}, blue for $5^{12}6^2$, red for $5^{12}6^3$, orange for $5^{12}6^4$, cyan for $4^15^{10}6^2$, purple for $4^15^{10}6^3$ and pink for $4^15^{10}6^4$).

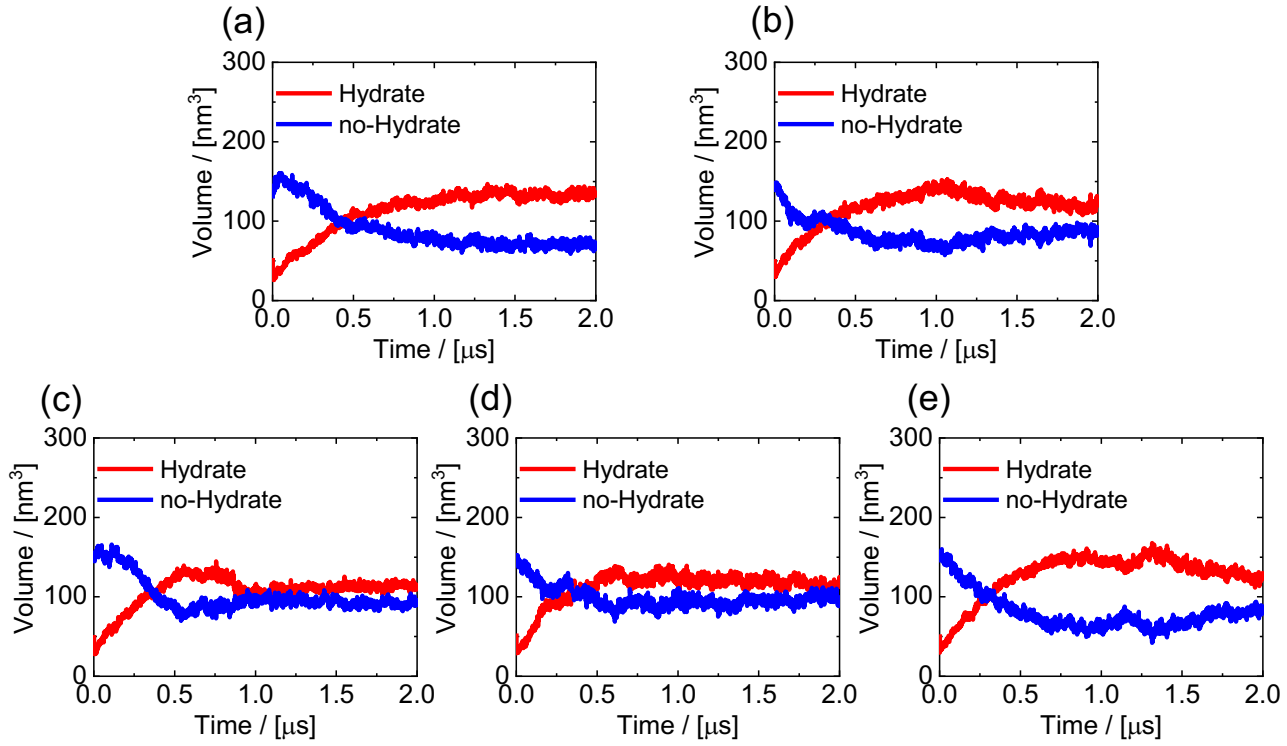

Figure S17. Evolution of the volume of the CO_2 hydrate solid in the (a) $H_{0\%Urea}$, (b) $H_{1.6\%Urea}$, (c) $H_{3\%Urea}$, (d) $H_{4.5\%Urea}$, and (e) $H_{6\%Urea}$ systems.

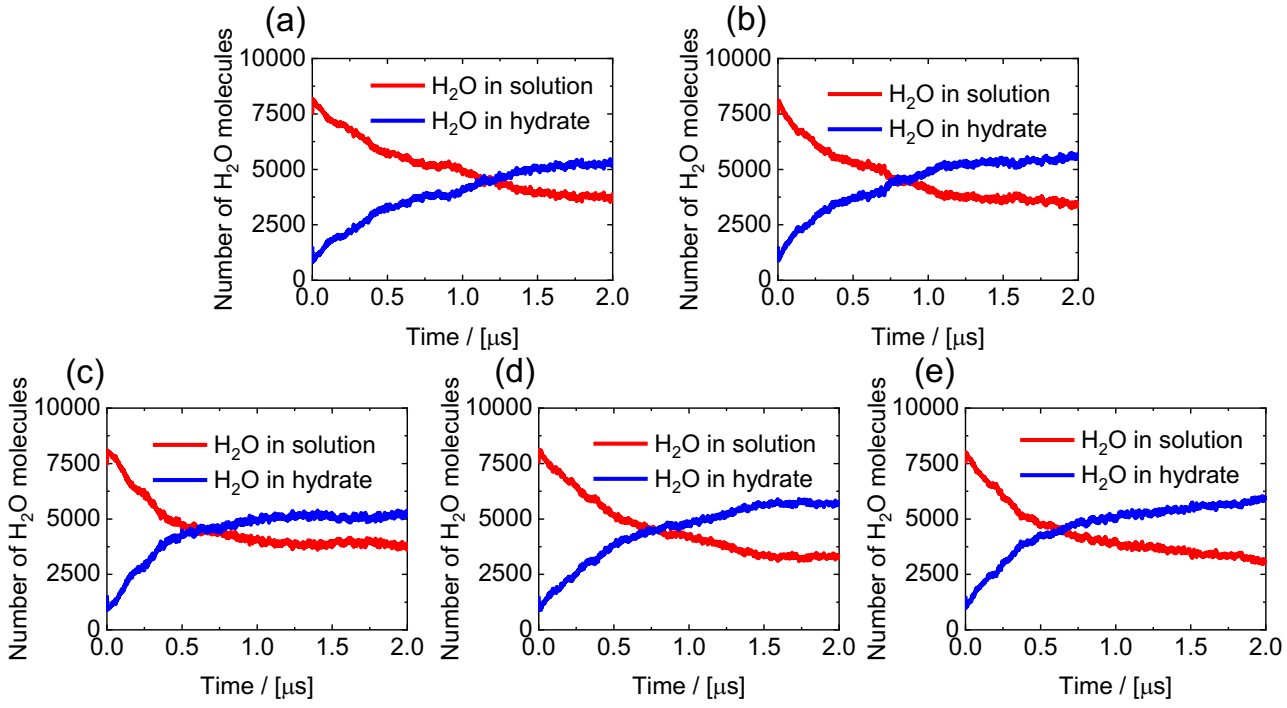

Figure S18. Evolution of the number of H_2O molecules in hydrate and solution in the (a) $H_{0\%Urea}$, (b) $H_{1.6\%Urea}$, (c)

$H_{3\%Urea}$, (d) $H_{4.5\%Urea}$, and (e) $H_{6\%Urea}$ systems.

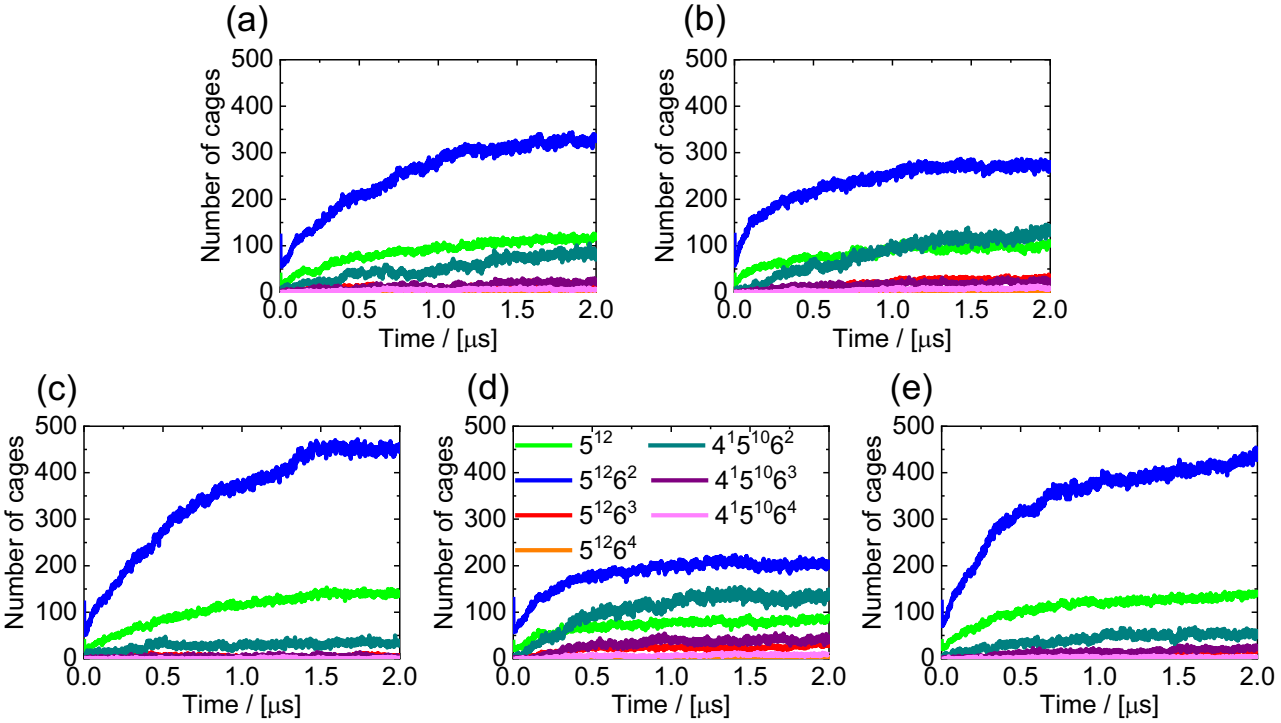

Figure S19. Evolution of the number of CO_2 hydrate cages in the (a) $H_{0\%Urea}$, (b) $H_{1.6\%Urea}$, (c) $H_{3\%Urea}$, (d) $H_{4.5\%Urea}$, and (e) $H_{6\%Urea}$ systems.

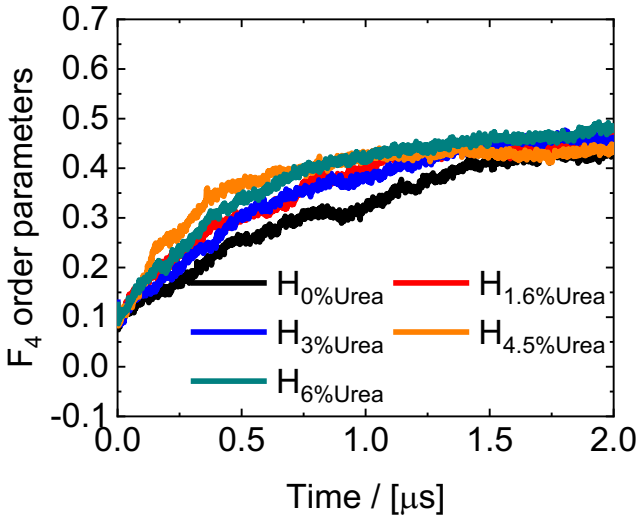

Figure S20. The evolution of the F_4 order parameter for the different five systems, *i.e.,* $H_{0\%Urea}$, $H_{1.6\%Urea}$, $H_{3\%Urea}$, $H_{4.5\%Urea}$, and $H_{6\%Urea}$ systems.

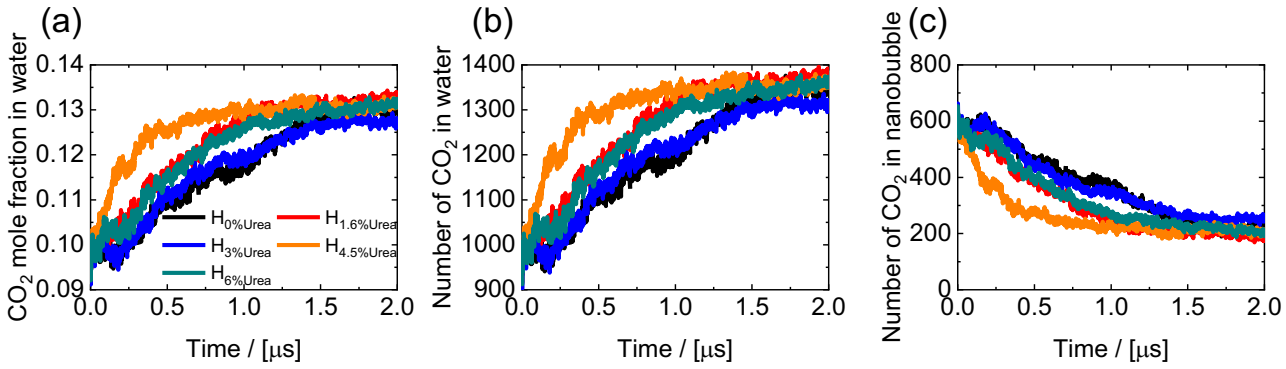

Figure S21. Evolution of (a) CO_2 mole fraction in water (x_{CO2}), number of CO_2 molecules (b) in water, and (c) in nanobubble for the different five systems, *i.e.,* $H_{0\%Urea}$, $H_{1.6\%Urea}$, $H_{3\%Urea}$, $H_{4.5\%Urea}$, and $H_{6\%Urea}$ systems.

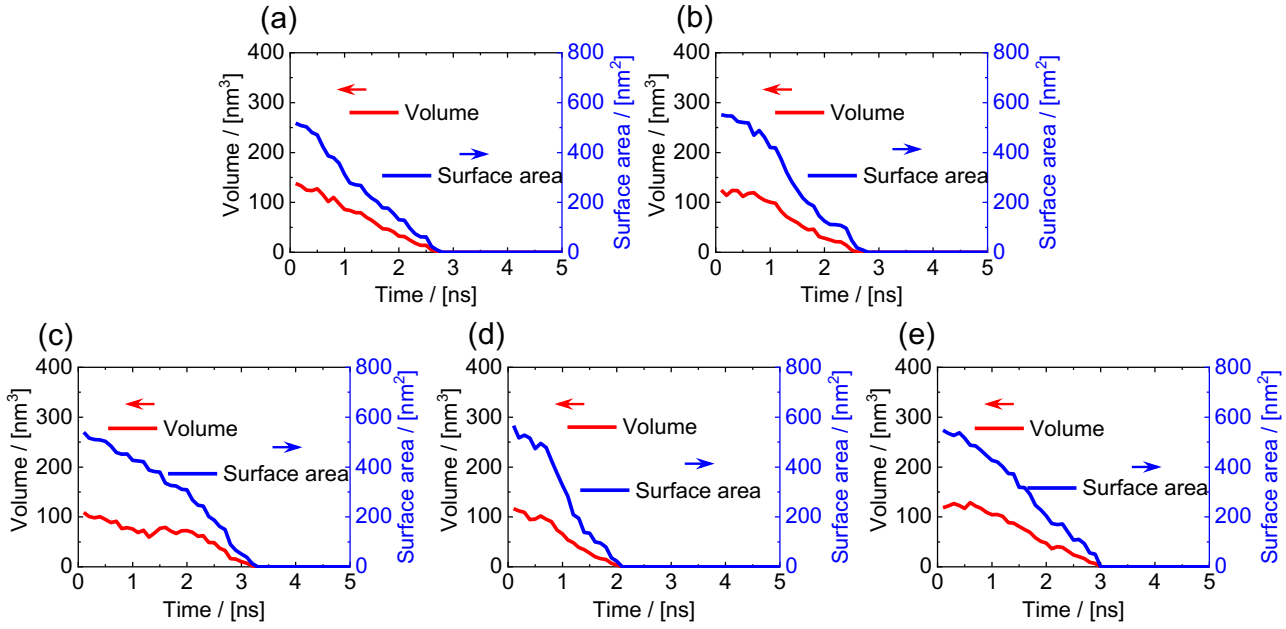

Figure S22. Evolution of the volume/surface area of CO_2 hydrate solid in the (a) $H_{0\%Urea}$, (b) $H_{1.6\%Urea}$, (c) $H_{3\%Urea}$, (d) $H_{4.5\%Urea}$, and (e) $H_{6\%Urea}$ systems.

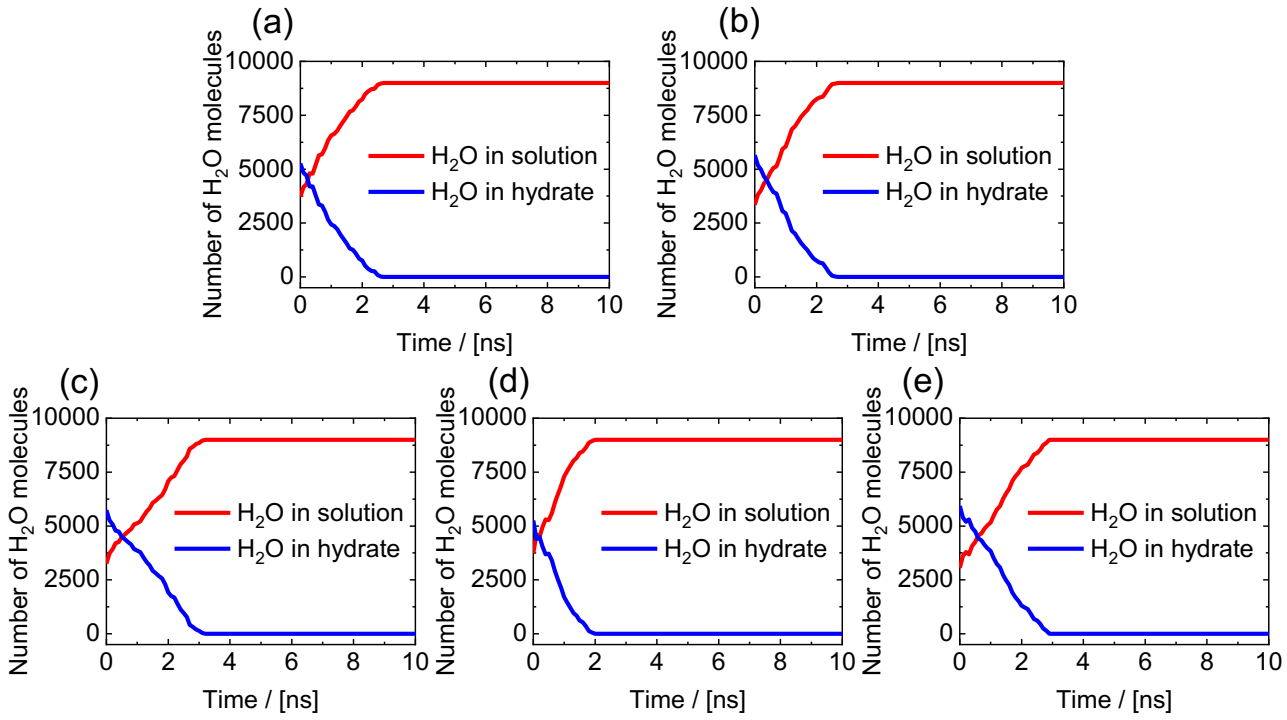

Figure S23. Evolution of the number of H_2O molecules in hydrate and solution in the (a) $H_{0\%Urea}$, (b) $H_{1.6\%Urea}$, (c) $H_{3\%Urea}$, (d) $H_{4.5\%Urea}$, and (e) $H_{6\%Urea}$ systems.

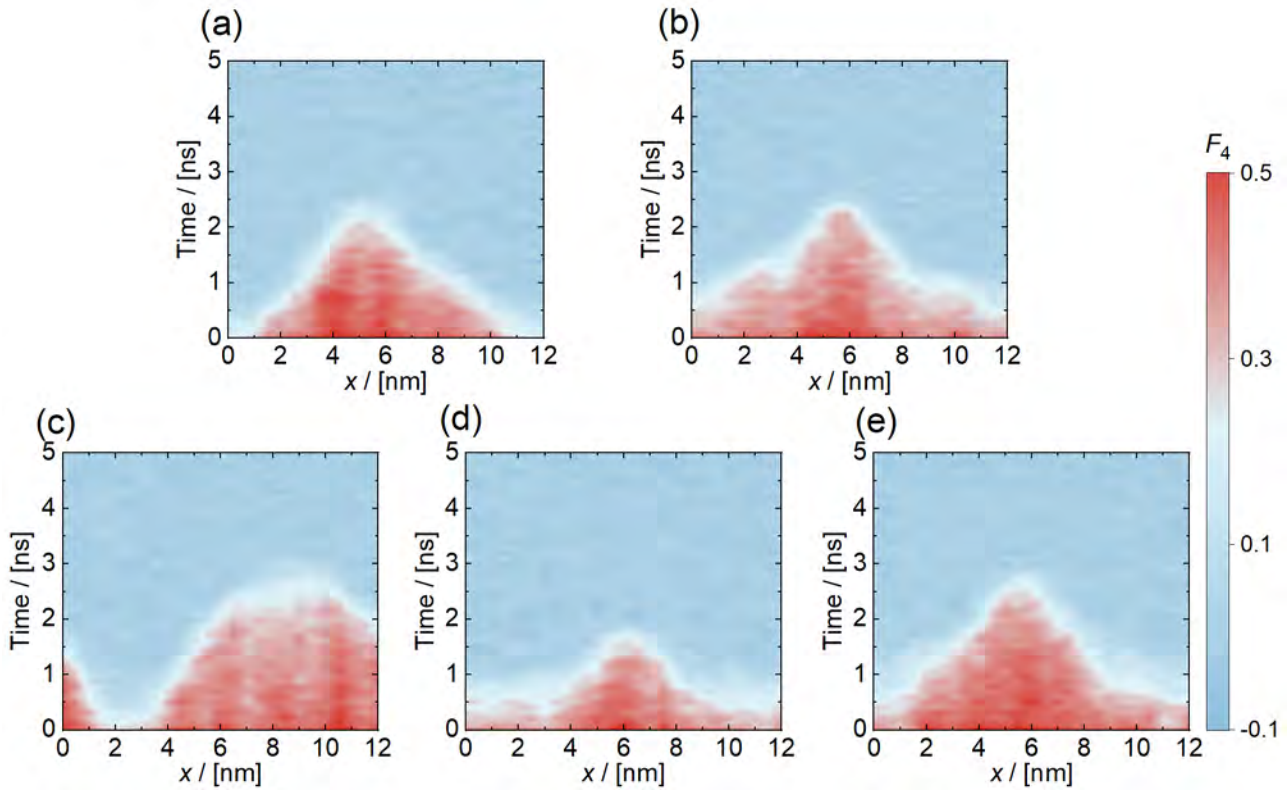

Figure S24. Evolution of the F_4 order parameter along the x-axis in the (a) $H_{0\%Urea}$, (b) $H_{1.6\%Urea}$, (c) $H_{3\%Urea}$, (d)

$H_{4.5\%Urea}$, and (e) $H_{6\%Urea}$ systems.

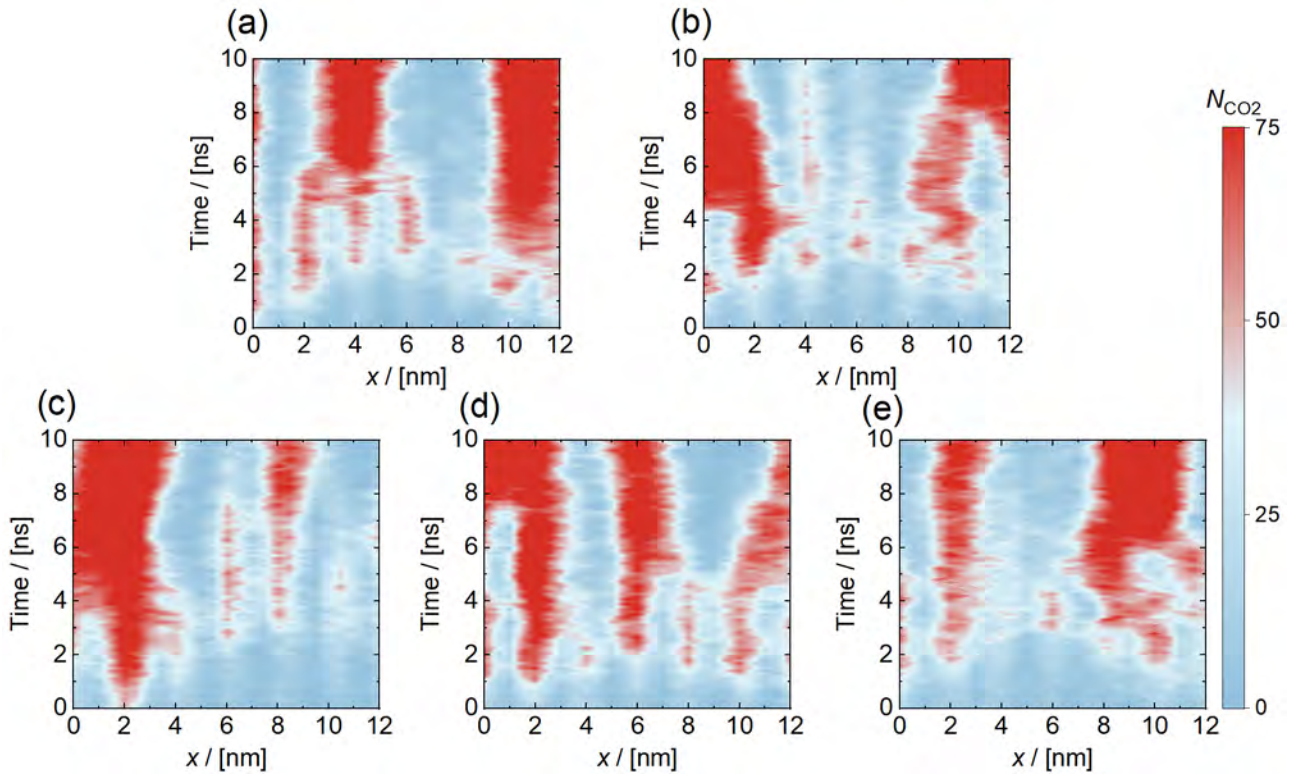

Figure S25. Evolution of the number of CO_2 in the nanobubbles (N_{CO2}) along the x-axis in the (a) $H_{0\%Urea}$, (b) $H_{1.6\%Urea}$, (c) $H_{3\%Urea}$, (d) $H_{4.5\%Urea}$, and (e) $H_{6\%Urea}$ systems.

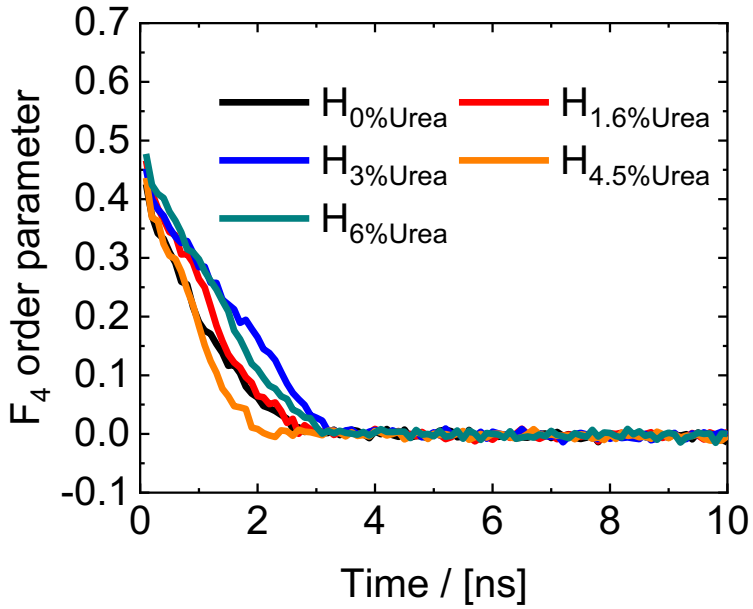

Figure S26. Evolution of the F_4 order parameter for the different five systems, *i.e.,* $H_{0\%Urea}$, $H_{1.6\%Urea}$, $H_{3\%Urea}$,

$H_{4.5\%Urea}$, and $H_{6\%Urea}$ systems.

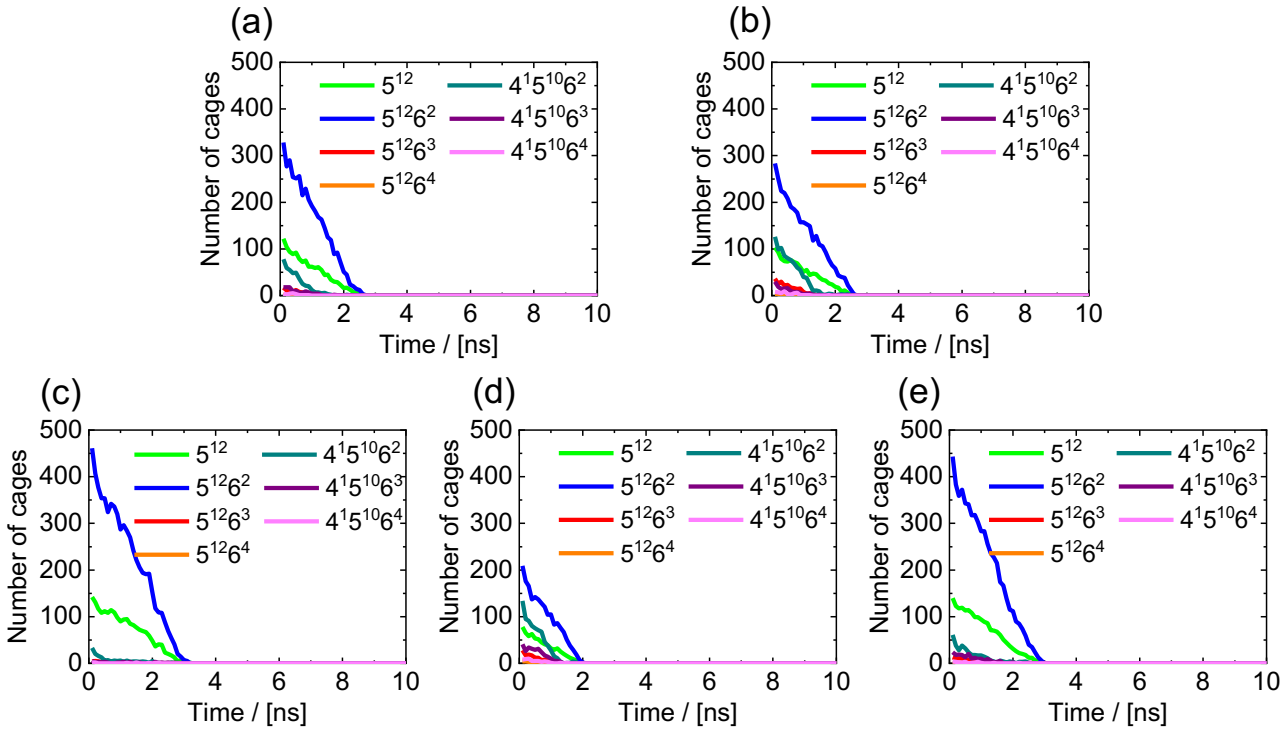

Figure S27. Evolution of the number of CO_2 hydrate cages in the (a) $H_{0\%Urea}$, (b) $H_{1.6\%Urea}$, (c) $H_{3\%Urea}$, (d) $H_{4.5\%Urea}$, and (e) $H_{6\%Urea}$ systems.

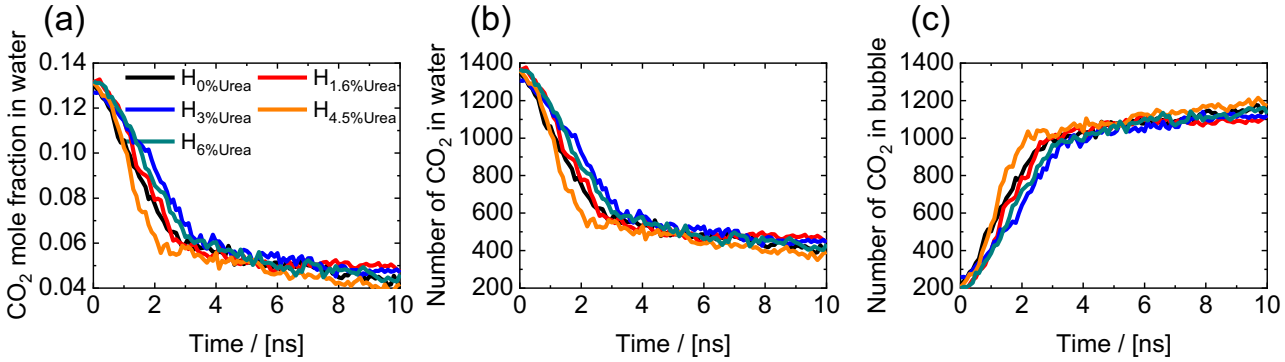

Figure S28. Evolution of (a) CO_2 mole fraction in water (x_{CO2}), number of CO_2 molecules (b) in water, and (c) in nanobubble for the different five systems, *i.e.,* $H_{0\%Urea}$, $H_{1.6\%Urea}$, $H_{3\%Urea}$, $H_{4.5\%Urea}$, and $H_{6\%Urea}$ systems.

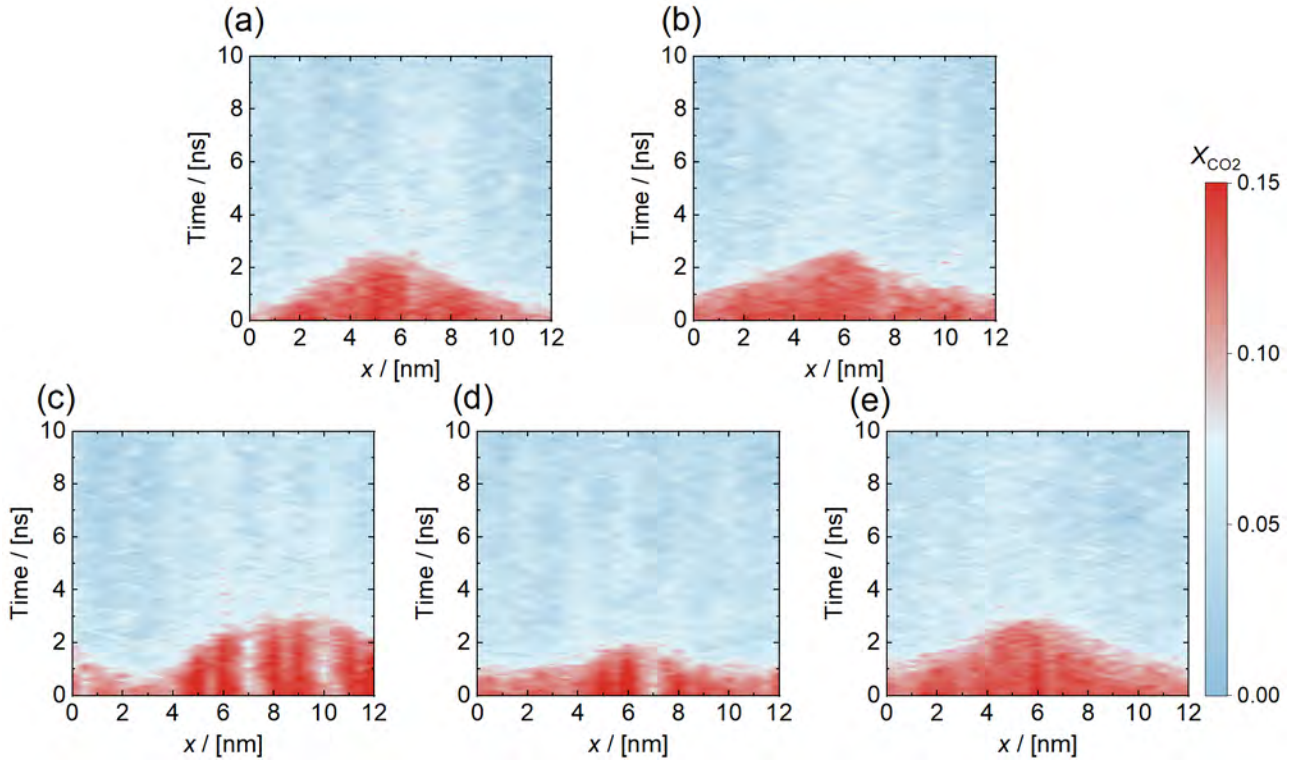

Figure S29. Evolution of the CO_2 mole fraction in water (x_{CO2}) for solutions along the x-axis in the (a) $H_{0\%Urea}$, (b) $H_{1.6\%Urea}$, (c) $H_{3\%Urea}$, (d) $H_{4.5\%Urea}$, and (e) $H_{6\%Urea}$ systems.

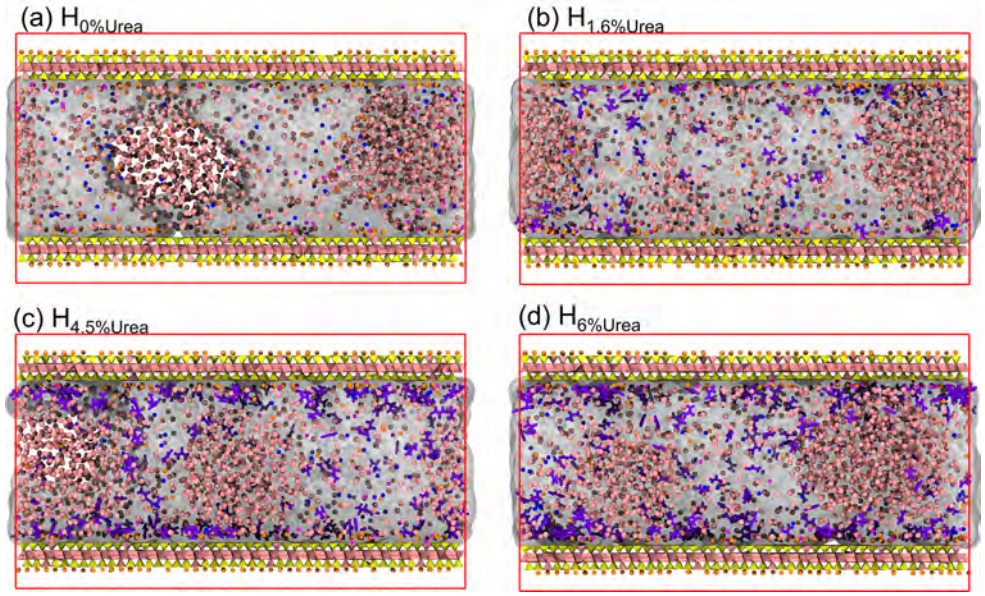

Figure S30. Dissociation snapshots at the end of the dissociation simulation (at the 10 ns) for the z-x plane in the different simulations: (a) $H_{0\%Urea}$, (b) $H_{1.6\%Urea}$, (c) $H_{4.5\%Urea}$, and (d) $H_{6\%Urea}$ systems. Illite are displayed as polyhedral, *i.e.,* yellow (Si atom), and pink (Al atom). Pink, blue, magenta, orange, and violet represent CO_2, Cl^-, Na^+, K^+, and urea, respectively.

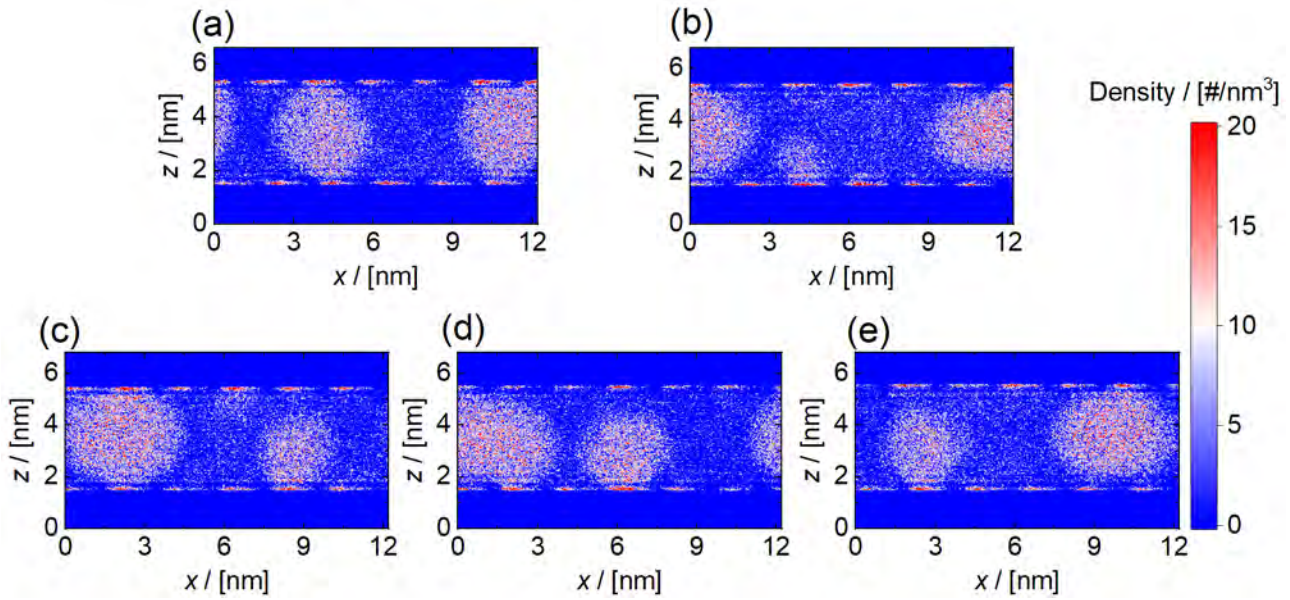

Figure S31. Number density distribution of CO_2 molecules for the last 2 ns of the dissociation process in the (a) $H_{0\%Urea}$, (b) $H_{1.6\%Urea}$, (c) $H_{3\%Urea}$, (d) $H_{4.5\%Urea}$, and (e) $H_{6\%Urea}$ systems.

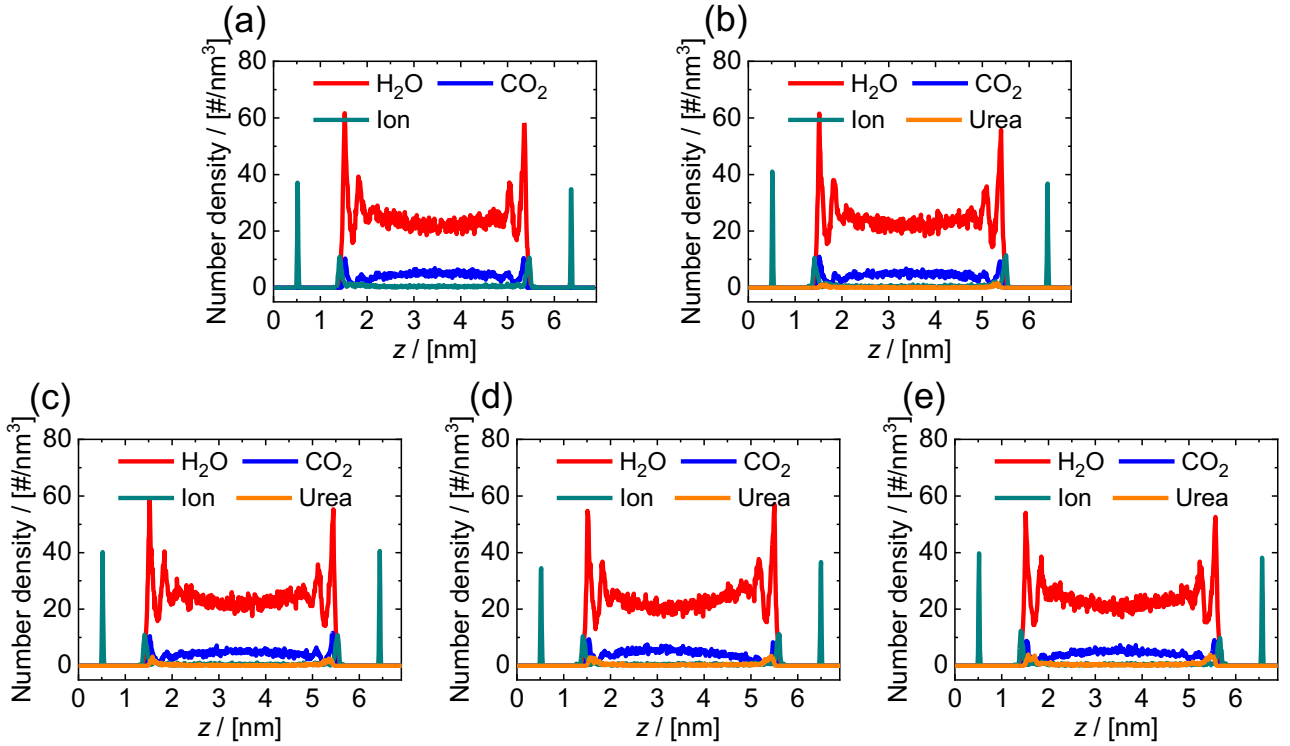

Figure S32. Number density distribution of H_2O, CO_2, ions, and urea molecules along the z-axis for 9 - 10 ns of the dissociation process for the (a) $H_{0\%Urea}$, (b) $H_{1.6\%Urea}$, (c) $H_{3\%Urea}$, (d) $H_{4.5\%Urea}$, and (e) $H_{6\%Urea}$ systems.

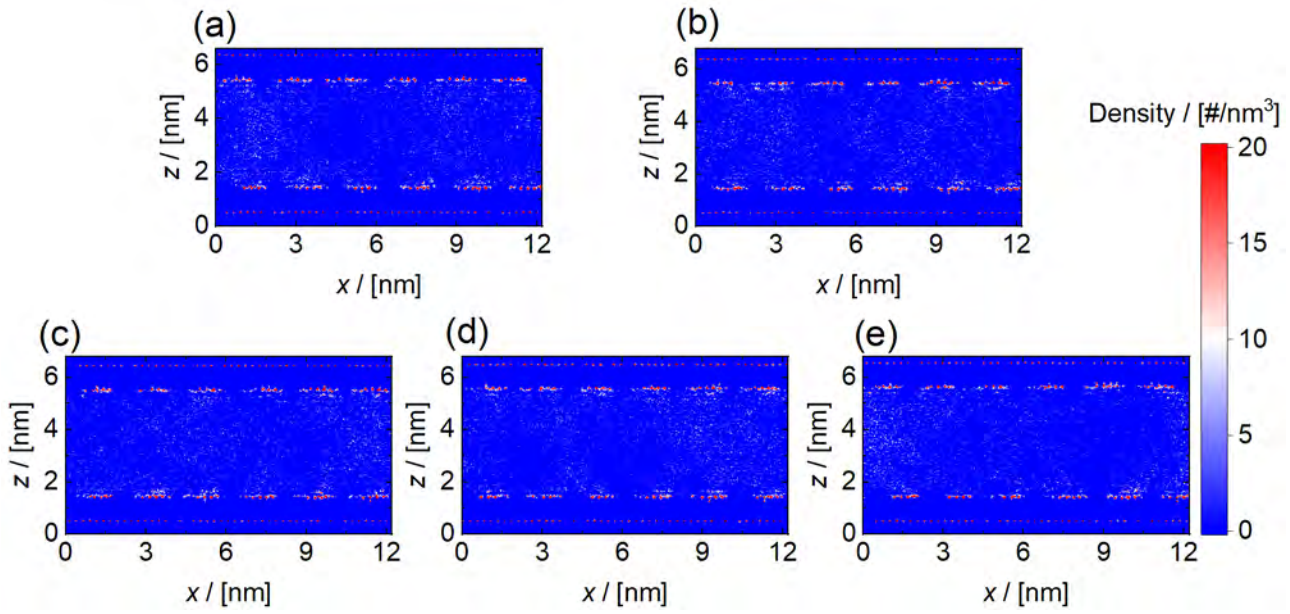

Figure S33. Number density distribution of ions for the last 2 ns of the dissociation process in the (a) $H_{0\%Urea}$, (b) $H_{1.6\%Urea}$, (c) $H_{3\%Urea}$, (d) $H_{4.5\%Urea}$, and (e) $H_{6\%Urea}$ systems.

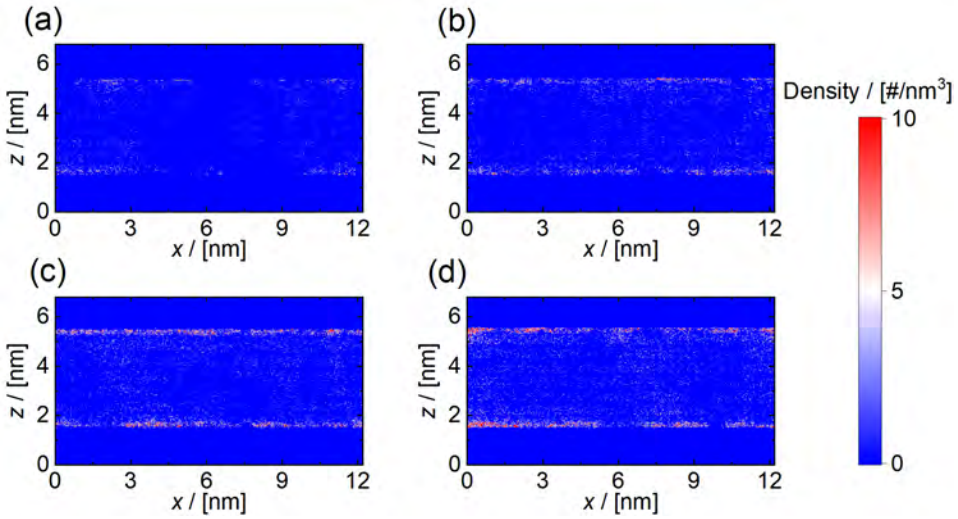

Figure S34. Number density distribution of urea molecules for the last 2 ns of the dissociation process in the (a) $H_{1.6\%Urea}$, (b) $H_{3\%Urea}$, (c) $H_{4.5\%Urea}$, and (d) $H_{6\%Urea}$ systems.

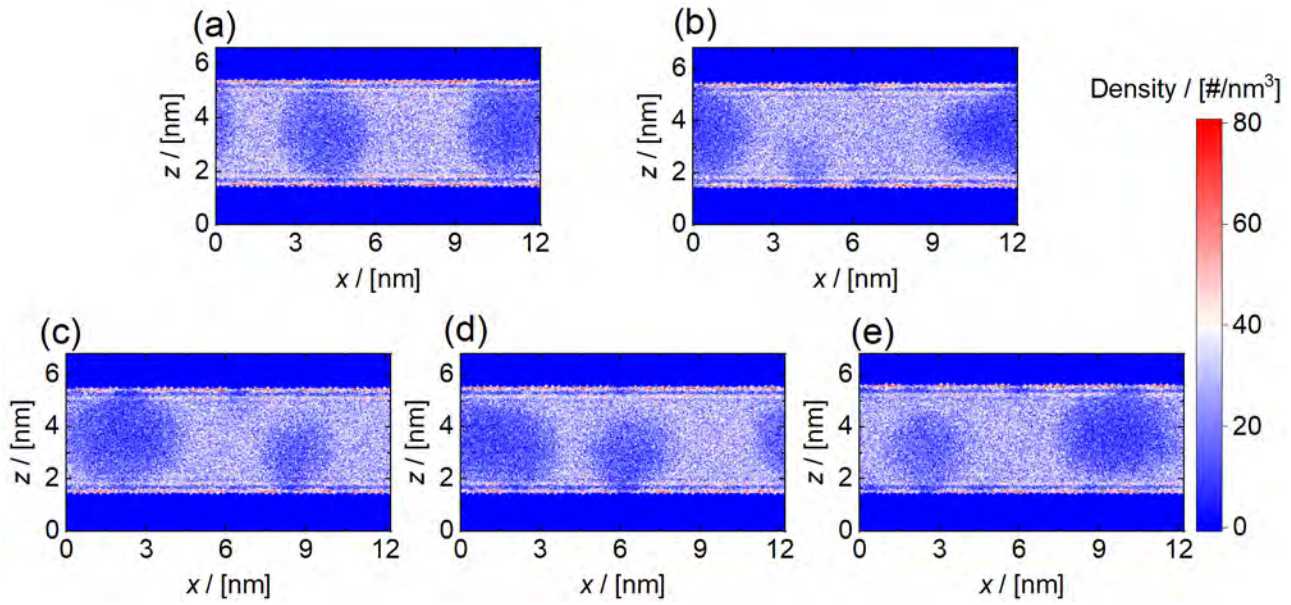

Figure S35. Number density distribution of H_2O molecules for the last 2 ns of the dissociation process in the (a) $H_{0\%Urea}$, (b) $H_{1.6\%Urea}$, (c) $H_{3\%Urea}$, (d) $H_{4.5\%Urea}$, and (e) $H_{6\%Urea}$ systems.

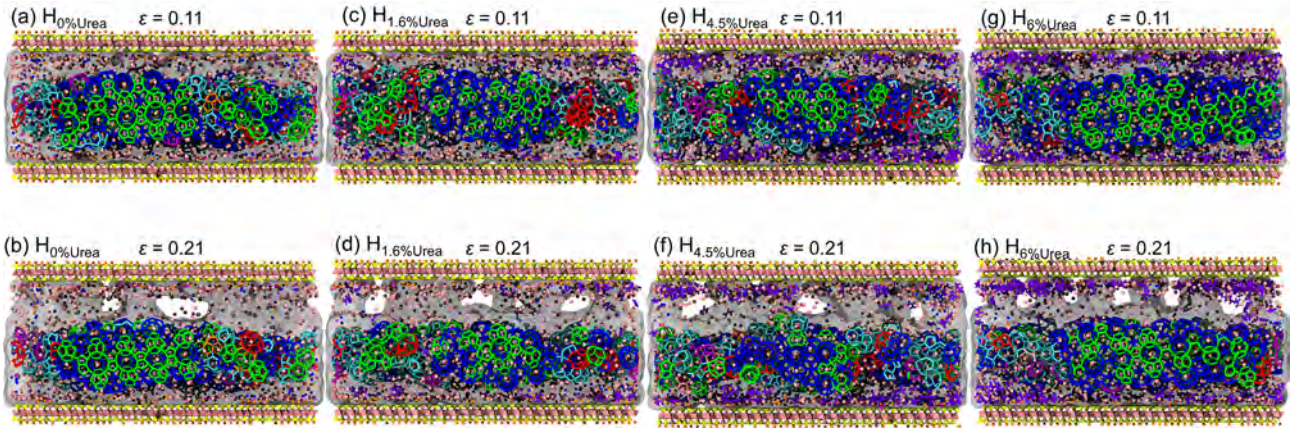

Figure S36. Snapshots of CO_2 hydrate-illite interface under tensile strain (ε) in the (a-b) $H_{0\%Urea}$, (c-d) $H_{1.6\%Urea}$, (e-f) $H_{4.5\%Urea}$, and (g-f) $H_{6\%Urea}$ systems. Illite is displayed as polyhedral, *i.e.,* yellow (Si atom), and pink (Al atom). Pink, blue, magenta, orange, and violet represent CO_2, Cl^-, Na^+, K^+, and urea, respectively. Hydrate cages are shown as sticks in various colors (green for 5^{12}, blue for $5^{12}6^2$, red for $5^{12}6^3$, orange for $5^{12}6^4$, cyan for $4^15^{10}6^2$, purple for $4^15^{10}6^3$ and pink for $4^15^{10}6^4$).

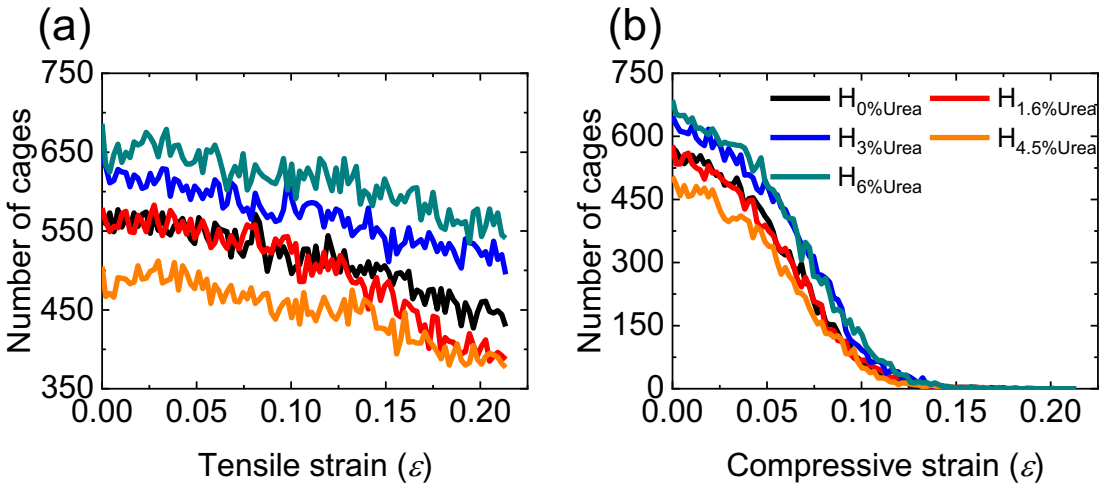

Figure S37. The evolution of the number of CO_2 hydrate cages under (a) tensile and (b) compressive strain (ε) for the different five systems, *i.e.,* $H_{0\%Urea}$, $H_{1.6\%Urea}$, $H_{3\%Urea}$, $H_{4.5\%Urea}$, and $H_{6\%Urea}$ systems.

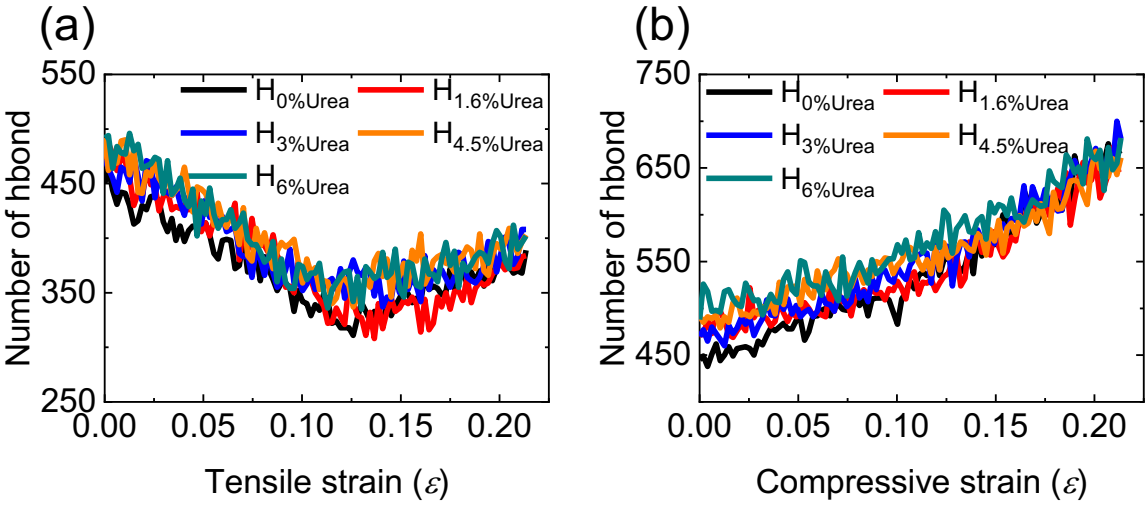

Figure S38. The evolution of the number of hydrogen bonds (hbonds) between urea/H_2O molecules and upper illite surface under (a) tensile and (b) compressive strain (ε) for the different five systems, *i.e.,* $H_{0\%Urea}$, $H_{1.6\%Urea}$, $H_{3\%Urea}$, $H_{4.5\%Urea}$, and $H_{6\%Urea}$ systems.

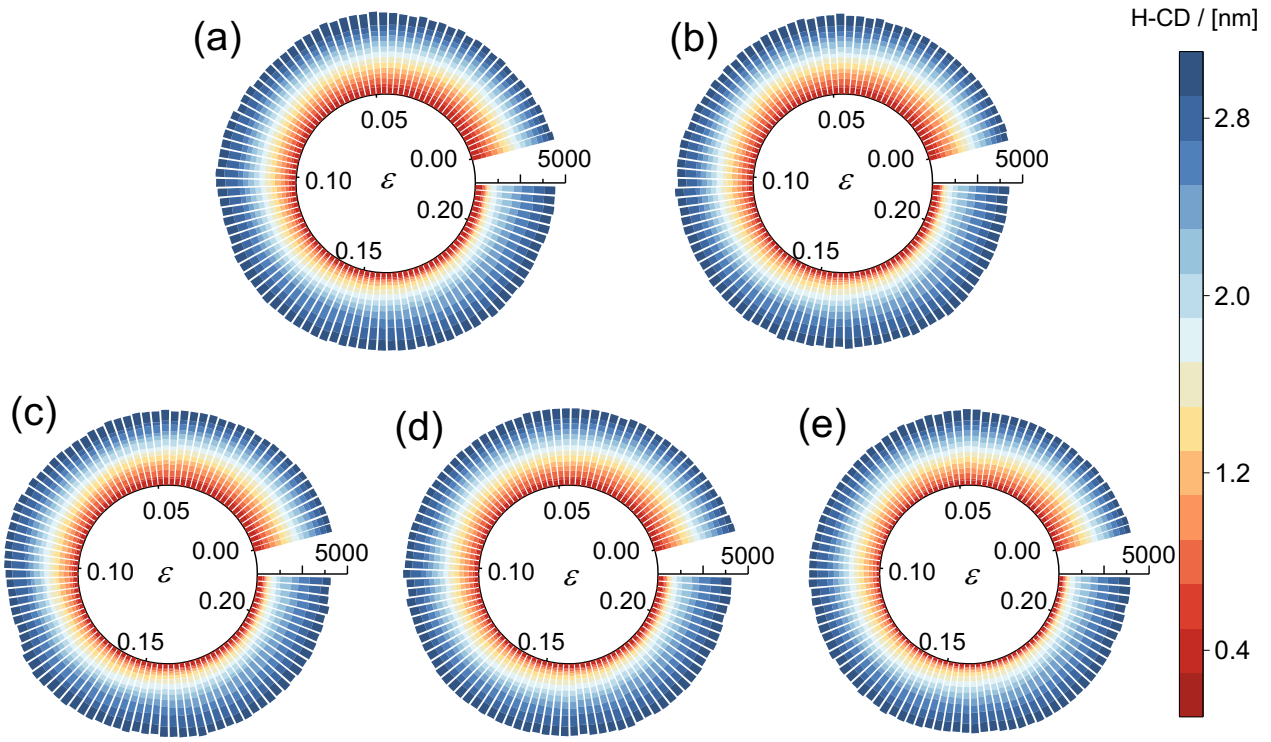

Figure S39. The number of hydrogen bonds at different distances from the upper illite surface (H-CD) under tensile strain (ε) in the (a) $H_{0\%Urea}$, (b) $H_{1.6\%Urea}$, (c) $H_{3\%Urea}$, (d) $H_{4.5\%Urea}$, and (e) $H_{6\%Urea}$ systems.

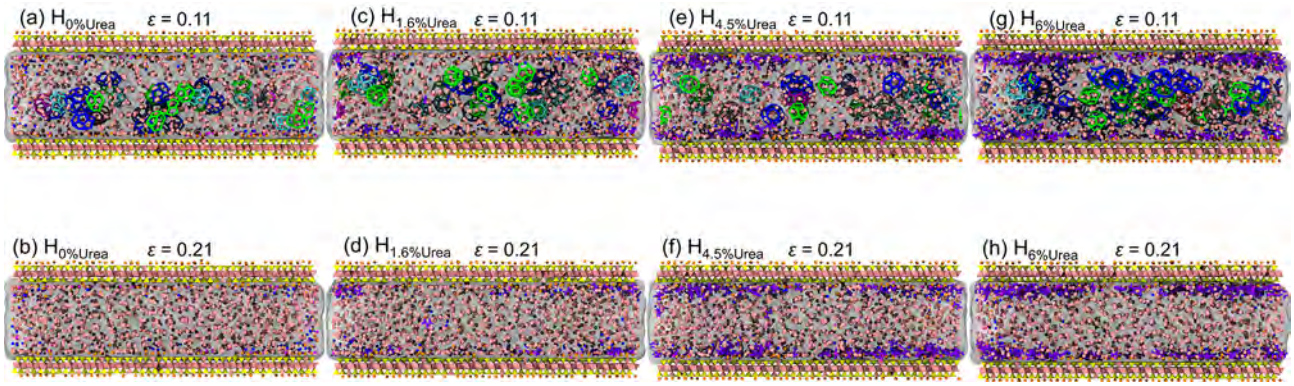

Figure S40. Snapshots of CO_2 hydrate-illite interface under compressive strain (ε) in the (a-b) $H_{0\%Urea}$, (c-d) $H_{1.6\%Urea}$, (e-f) $H_{4.5\%Urea}$, and (g-f) $H_{6\%Urea}$ systems. Illite are displayed as polyhedral, *i.e.,* yellow (Si atom), and pink (Al atom). Pink, blue, magenta, orange, and violet represent CO_2, Cl^-, Na^+, K^+, and urea, respectively. Hydrate cages are shown as sticks in various colors (green for 5^{12}, blue for $5^{12}6^2$, red for $5^{12}6^3$, orange for $5^{12}6^4$, cyan for $4^15^{10}6^2$, purple for $4^15^{10}6^3$ and pink for $4^15^{10}6^4$).

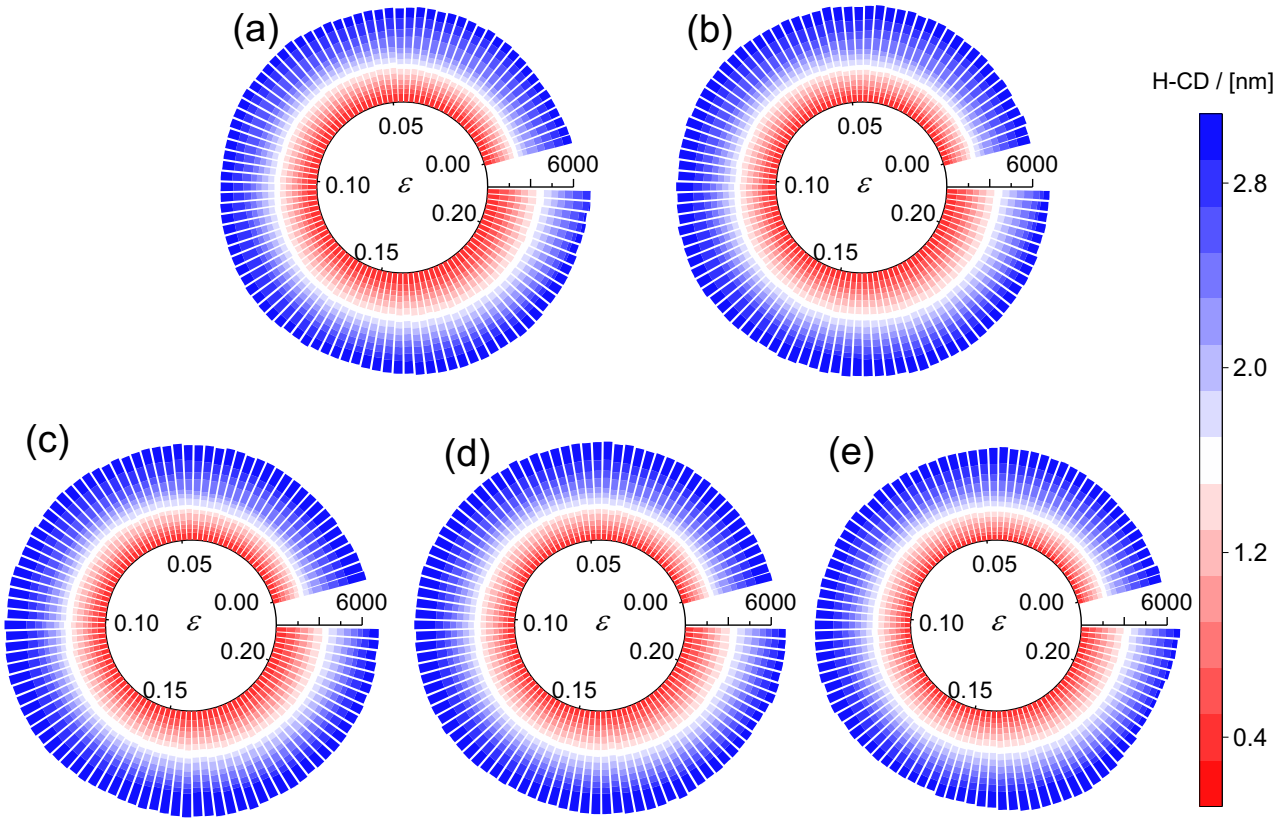

Figure S41. Number of hydrogen bonds at different distances from the upper illite surface under compressive strains (ε) in the (a) $H_{0\%Urea}$, (b) $H_{1.6\%Urea}$, (c) $H_{3\%Urea}$, (d) $H_{4.5\%Urea}$, and (e) $H_{6\%Urea}$ systems.

Supporting Videos

Video S1. Growth process of CO_2 hydrate in oceanic sediments for the $H_{3\%Urea}$ system. Illite is displayed as polyhedral, *i.e.,* yellow (Si atom) and pink (Al atom). Pink, blue, magenta, orange, and violet represent CO_2, Cl^-, Na^+, K^+, and urea, respectively. Hydrate cages are shown as sticks in various colors (green for 5^{12}, blue for $5^{12}6^2$, red for $5^{12}6^3$, orange for $5^{12}6^4$, cyan for $4^15^{10}6^2$, purple for $4^15^{10}6^3$ and pink for $4^15^{10}6^4$).

Video S2. Dissociation process of CO_2 hydrate in oceanic sediments for the $H_{3\%Urea}$ system. Illite is displayed as polyhedral, *i.e.,* yellow (Si atom) and pink (Al atom). Pink, blue, magenta, orange, and violet represent CO_2, Cl^-, Na^+, K^+, and urea, respectively. Hydrate cages are shown as sticks in various colors (green for 5^{12}, blue for $5^{12}6^2$, red for $5^{12}6^3$, orange for $5^{12}6^4$, cyan for $4^15^{10}6^2$, purple for $4^15^{10}6^3$ and pink for $4^15^{10}6^4$).

Video S3. Tension process of CO_2 hydrate-illite interface in oceanic sediments for the $H_{3\%Urea}$ system. Illite is displayed as polyhedral, *i.e.,* yellow (Si atom) and pink (Al atom). Pink, blue, magenta, orange, and violet represent CO_2, Cl^-, Na^+, K^+, and urea, respectively. Hydrate cages are shown as sticks in various colors (green for 5^{12}, blue for $5^{12}6^2$, red for $5^{12}6^3$, orange for $5^{12}6^4$, cyan for $4^15^{10}6^2$, purple for $4^15^{10}6^3$ and pink for $4^15^{10}6^4$).

Video S4. Compression process of CO_2 hydrate-illite interface in oceanic sediments for the $H_{3\%Urea}$ system. Illite is displayed as polyhedral, *i.e.,* yellow (Si atom) and pink (Al atom). Pink, blue, magenta, orange, and violet represent CO_2, Cl^-, Na^+, K^+, and urea, respectively. Hydrate cages are shown as sticks in various colors (green for 5^{12}, blue for $5^{12}6^2$, red for $5^{12}6^3$, orange for $5^{12}6^4$, cyan for $4^15^{10}6^2$, purple for $4^15^{10}6^3$ and pink for $4^15^{10}6^4$).

Supporting Reference

(1) Downs, R. T.; Hall-Wallace, M. The crystal structure database. *Am. Mineral.* **2003**, *88*, 247-250.

(2) Fang, B.; Lü, T.; Li, W.; Moultos, O. A.; Vlugt, T. J. H.; Ning, F. Microscopic insights into poly-and mono-crystalline methane hydrate dissociation in Na-montmorillonite pores at static and dynamic fluid conditions. *Energy* **2024**, *288*, 129755.

(3) Abascal, J. L.; Sanz, E.; Garcia Fernandez, R.; Vega, C. A potential model for the study of ices and amorphous water: TIP4P/Ice. *J. Chem. Phys.* **2005**, *122*, 234511.

(4) Potoff, J. J.; Siepmann, J. I. Vapor–liquid equilibria of mixtures containing alkanes, carbon dioxide, and nitrogen. *AlChE J.* **2001**, *47*, 1676-1682.

(5) Jorgensen, W. L.; Maxwell, D. S.; TiradoRives, J. Development and testing of the OPLS all-atom force field on conformational energetics and properties of organic liquids. *J. Am. Chem. Soc.* **1996**, *118*, 11225-11236.

(6) Cygan, R. T.; Liang, J. J.; Kalinichev, A. G. Molecular models of hydroxide, oxyhydroxide, and clay phases and

the development of a general force field. *J. Phys. Chem. B* **2004**, *108*, 1255-1266.

(7) Abraham, M. J.; Murtola, T.; Schulz, R.; Páll, S.; Smith, J. C.; Hess, B.; Lindahl, E. GROMACS: High performance molecular simulations through multi-level parallelism from laptops to supercomputers. *SoftwareX* **2015**, *1*, 19-25.

(8) Nosé, S. A Molecular-Dynamics Method for Simulations in the Canonical Ensemble. *Mol. Phys.* **1984**, *52*, 255-268.

(9) Bussi, G.; Donadio, D.; Parrinello, M. Canonical sampling through velocity rescaling. *J Chem Phys* **2007**, *126*, 014101.

(10) Berendsen, H. J. C.; Postma, J. P. M.; Vangunsteren, W. F.; Dinola, A.; Haak, J. R. Molecular-Dynamics with Coupling To an External Bath. *J. Chem. Phys.* **1984**, *81*, 3684-3690.

(11) Parrinello, M.; Rahman, A. Crystal-Structure and Pair Potentials - a Molecular-Dynamics Study. *Phys. Rev. Lett.* **1980**, *45*, 1196-1199.

(12) Jacobson, L. C.; Hujo, W.; Molinero, V. Thermodynamic stability and growth of guest-free clathrate hydrates: a low-density crystal phase of water. *J. Phys. Chem. B* **2009**, *113*, 10298-10307.

(13) Báez, L. A.; Clancy, P. Computer Simulation of the Crystal Growth and Dissolution of Natural Gas Hydrates a. *Ann. N.Y. Acad. Sci.* **1994**, *715*, 177-186.

(14) Humphrey, W.; Dalke, A.; Schulten, K. VMD: visual molecular dynamics. *J Mol Graph* **1996**, *14*, 33-38, 27-38.